

AD-A193 169

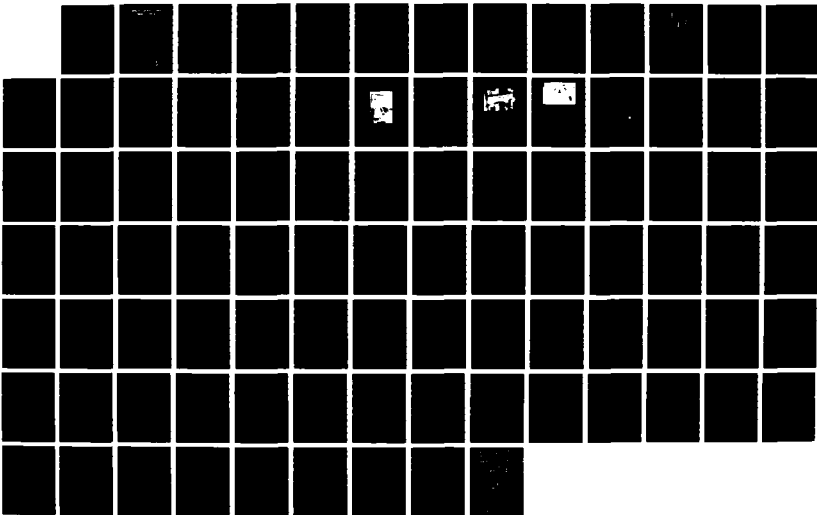
A TRANSITION RADIATION EXPERIMENT TO MEASURE THE
ELECTRON BEAM MODULATION. (U) NAVAL POSTGRADUATE SCHOOL
MONTEREY CA J E JOYNSON DEC 87

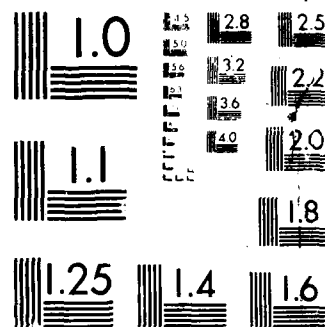
1/1

UNCLASSIFIED

F/G 9/3

NL





MICROCOPY RESOLUTION TEST CHART
NATIONAL BUREAU OF STANDARDS-1963-A

AD-A195 169

DTIC FILE COPY

2

NAVAL POSTGRADUATE SCHOOL

Monterey, California



THESIS

A TRANSITION RADIATION EXPERIMENT TO MEASURE
THE ELECTRON BEAM MODULATION INDUCED BY
THE FREE ELECTRON LASER: A DESIGN STUDY

by

Jack E. Joynson

December 1987

Thesis Co-Advisors:

Fred R. Buskirk
Xavier K. Maruyama

Approved for public release; distribution is unlimited

DTIC
ELECTE
JUN 03 1988
S H D

86

0

1

2

3

4

5

REPORT DOCUMENTATION PAGE

ADA195169

1a. REPORT SECURITY CLASSIFICATION UNCLASSIFIED			1b. RESTRICTIVE MARKINGS		
2a. SECURITY CLASSIFICATION AUTHORITY			3. DISTRIBUTION/AVAILABILITY OF REPORT Approved for public release; distribution is unlimited		
2b. DECLASSIFICATION/DOWNGRADING SCHEDULE					
4. PERFORMING ORGANIZATION REPORT NUMBER(S)			5. MONITORING ORGANIZATION REPORT NUMBER(S)		
6a. NAME OF PERFORMING ORGANIZATION Naval Postgraduate School		6b. OFFICE SYMBOL (If applicable) Code 61		7a. NAME OF MONITORING ORGANIZATION Naval Postgraduate School	
6c. ADDRESS (City, State, and ZIP Code) Monterey, California 93943-5000			7b. ADDRESS (City, State, and ZIP Code) Monterey, California 93943-5000		
8a. NAME OF FUNDING/SPONSORING ORGANIZATION		8b. OFFICE SYMBOL (If applicable)		9. PROCUREMENT INSTRUMENT IDENTIFICATION NUMBER	
8c. ADDRESS (City, State, and ZIP Code)			10. SOURCE OF FUNDING NUMBERS		
			PROGRAM ELEMENT NO.	PROJECT NO.	TASK NO.
			WORK UNIT ACCESSION NO.		
11. TITLE (Include Security Classification) A TRANSITION RADIATION EXPERIMENT TO MEASURE THE ELECTRON BEAM MODULATION INDUCED BY THE FREE ELECTRON LASER: A DESIGN STUDY					
12. PERSONAL AUTHOR(S) Jovnson, Jack E.					
13a. TYPE OF REPORT Master's Thesis		13b. TIME COVERED FROM TO		14. DATE OF REPORT (Year, Month, Day) 1987, December	
				15. PAGE COUNT 89	
16. SUPPLEMENTARY NOTATION					
17. COSATI CODES			18. SUBJECT TERMS (Continue on reverse if necessary and identify by block number)		
FIELD	GROUP	SUB-GROUP	Electron Beam Diagnostics; Free Electron Lasers; Electron Beams; Modulated Beam; Transition Radiation; TRANSPORT <u>Theses</u>		
19. ABSTRACT (Continue on reverse if necessary and identify by block number) The modulated beam of the free electron laser when passed through a thin target should produce strong transition radiation. The measurement of the transition radiation is a direct measurement of the electron beam modulation in the free electron laser. A transition radiation experiment using the Stanford MKIII Infrared Free Electron Laser (IRFEL) has been proposed. The analysis has centered on TRANSPORT, a computer program used for designing charged particle beam systems. The MKIII IRFEL wiggler exit bending magnet system was modeled using TRANSPORT. Analysis reveals that the transverse emittance and momentum spread characteristics will cause the modulated beam to demodulate along the path of the central trajectory. A detector location 10 millimeters downstream of the first bending magnet is found suitable for the measurement of the electron beam modulation. For this case the thin					
20. DISTRIBUTION/AVAILABILITY OF ABSTRACT <input checked="" type="checkbox"/> UNCLASSIFIED/UNLIMITED <input type="checkbox"/> SAME AS RPT <input type="checkbox"/> DTIC USERS			21. ABSTRACT SECURITY CLASSIFICATION Unclassified		
22a. NAME OF RESPONSIBLE INDIVIDUAL Professor Fred R. Buskirk			22b. TELEPHONE (Include Area Code) (408) 646-2765		22c. OFFICE SYMBOL Code 61Bs

UNCLASSIFIED

SECURITY CLASSIFICATION OF THIS PAGE (When Data Entered)

#19 - ABSTRACT - (CONTINUED)

- ✓ foil must be rotated approximately 11.25 degrees about the y-axis to yield a minimum effective picobunch extent as seen by the thin foil. Alternate FEL systems are suggested for investigation.

Accession For	
NTIS GRA&I	<input checked="" type="checkbox"/>
DTIC TAB	<input type="checkbox"/>
Unannounced	<input type="checkbox"/>
Justification	
By	
Distribution/	
Availability Codes	
Dist	Avail and/or Special
A-1	



UNCLASSIFIED

SECURITY CLASSIFICATION OF THIS PAGE (When Data Entered)

Approved for Public Release; distribution is unlimited

A Transition Radiation Experiment to Measure
the Electron Beam Modulation Induced by
the Free Electron Laser: A Design Study

by

Jack E. Joynson
Lieutenant, United States Navy
B.S., United States Naval Academy, 1982

Submitted in partial fulfillment of the
requirements for the degree of

MASTER OF SCIENCE IN PHYSICS


from the

NAVAL POSTGRADUATE SCHOOL
December, 1987

Author:


Jack E. Joynson

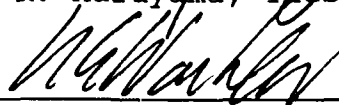
Approved By:



Fred R. Buskirk, Thesis Co-Advisor



Xavier K. Maruyama, Thesis Co-Advisor



Kai Woehler, Chairman,
Department of Physics



Gordon E. Schacher,
Dean of Science and Engineering

ABSTRACT

The modulated beam of the free electron laser when passed through a thin target should produce strong transition radiation. The measurement of the transition radiation is a direct measurement of the electron beam modulation in the free electron laser. A transition radiation experiment using the Stanford MKIII Infrared Free Electron Laser (IRFEL) has been proposed. The analysis has centered on TRANSPORT, a computer program used for designing charged particle beam systems. The MKIII IRFEL wiggler exit bending magnet system was modeled using TRANSPORT. Analysis reveals that the transverse emittance and momentum spread characteristics will cause the modulated beam to demodulate along the path of the central trajectory. A detector location 10 millimeters downstream of the first bending magnet is found suitable for the measurement of the electron beam modulation. For this case the thin foil must be rotated approximately 11.25 degrees about the y-axis to yield a minimum effective picobunch extent as seen by the thin foil. Alternate FEL systems are suggested for investigation.

TABLE OF CONTENTS

I.	INTRODUCTION -----	1
	A. OVERVIEW -----	1
	B. MODULATION OF THE ELECTRON BEAM -----	2
	C. WHAT IS TRANSITION RADIATION -----	8
II.	PROPOSED EXPERIMENT USING MKIII IRFEL -----	11
	A. EXPERIMENT PROPOSAL -----	11
	1. System Description -----	11
	2. Possible Detector Locations -----	15
	3. Hardware Design at Detector Locations ---	15
	B. ANALYSIS OF ELECTRON BEAM TRANSPORT EQUATIONS -----	17
	1. Buskirk System Equations -----	21
	2. TRANSPORT Equations -----	23
III.	RESULTS AND CONCLUSIONS -----	38
	APPENDIX A: BEAM TRANSPORT THEORY -----	42
	APPENDIX B: TRANSPORT-A COMPUTER PROGRAM USED FOR DESIGNING CHARGED PARTICLE BEAM SYSTEMS --	49
	LIST OF REFERENCES -----	79
	INITIAL DISTRIBUTION LIST -----	81

ACKNOWLEDGMENTS

I am grateful to all those who have contributed directly or indirectly to the completion of this thesis work. A special thanks to Professor Buskirk for the initial idea and development of this experiment; to Professor Maruyama for his untiring support as a "Suzuki" Thesis Co-Advisor; to Dr. Steve Benson for his overall cooperation and assistance concerning the MKIII IRFEL; to Dr. Arthur Paul of LLNL for his instruction in the matrix methods of TRANSPORT; to Dr Tom Knight and Dr Richard Helm of SLAC for their assistance in obtaining TRANSPORT for the Naval Postgraduate School; and to Don Snyder for his assistance in the experimental design apparatus required for the experiment.

I. INTRODUCTION

A. OVERVIEW

The electron beam from a free electron laser (FEL) offers the possibility of observing and using transition radiation (TR) at optical frequencies. After interacting with the wiggler and radiation fields, the electron beam becomes modulated in the axial direction at the lasing frequency [Ref. 1]. The axially modulated bunches (picobunches) could be passed through a thin foil producing the surface effect TR as illustrated in Figure 1-1.

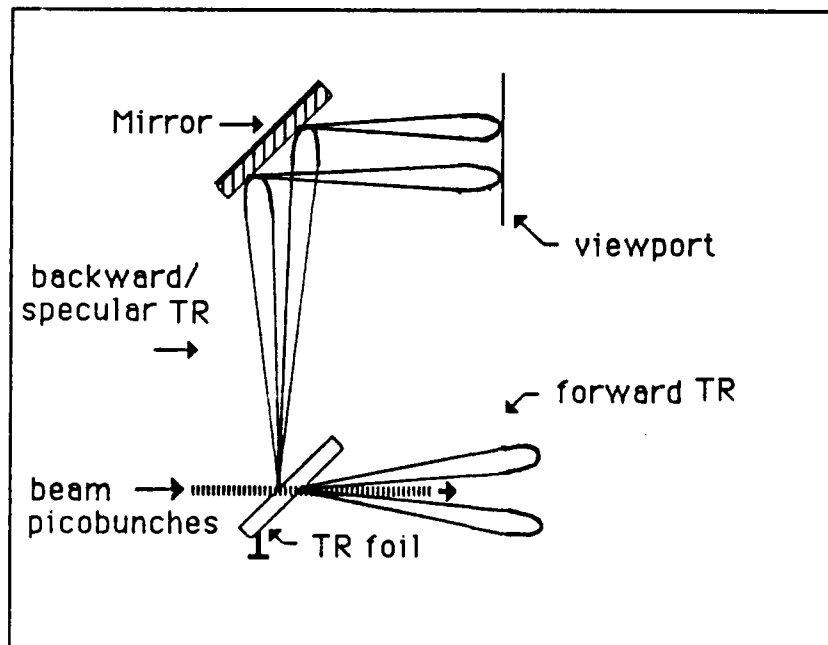


Figure 1-1 Transition Radiation (TR)

The axially modulated beam picobunches impact a thin foil of aluminum or mylar yielding forward and backward/specular TR [Ref. 2]. Both forms of radiation should be enhanced by coherent emission from all charges in the picobunch. The backward/specular TR is redirected to a viewing port/optical detector by a mirror. The resulting radiation could be used to diagnose the electron beam modulation [Ref. 1].

The TR power radiated per picobunch is found to be proportional to the charge of the picobunch squared. For a picobunch of approximately 10^6 electrons, the radiation intensity can easily be detected and measured with an optical detector. The axially modulated electron beam of the IRFEL, upon impact with the thin foil or multifoil, will generate coherent optical transition radiation. [Ref. 2]

B. MODULATION OF THE ELECTRON BEAM

The longitudinal bunching of the electron beam by the undulator of the free electron laser (FEL) is a result of the force acting on the individual particles by the electric field of the superimposed laser radiation. This effect on a single electron is examined in Figure 1-2 [Ref. 3]. This figure illustrates the fields and trajectories within the undulator of a FEL: an alternating magnetic field, a co-propagating laser electric field and an electron along a trajectory. The electric field of the laser is zero at position A. The electron experiences no force other than that of the undulator's magnetic field, which will bend it

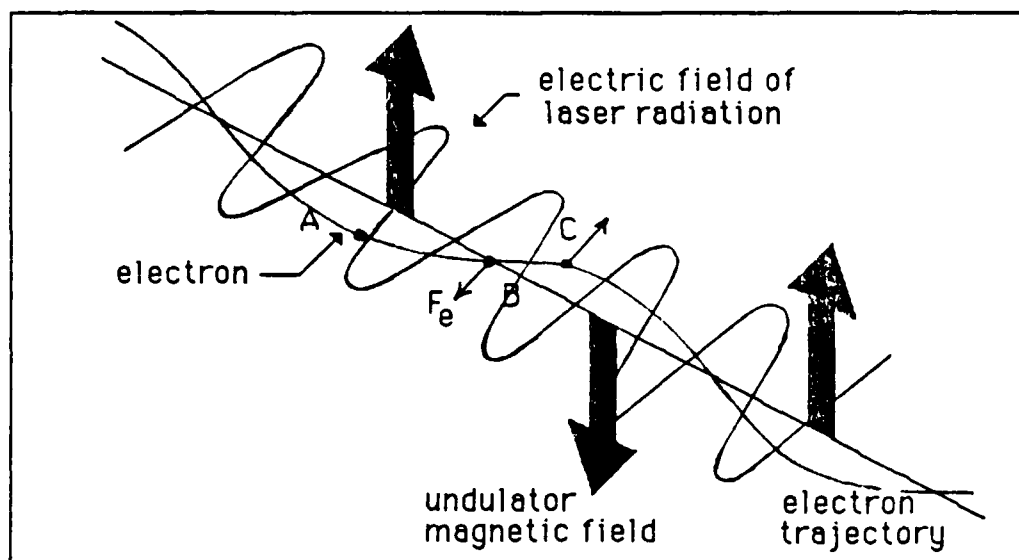


Figure 1-2 Longitudinal Bunching of the Electron Beam

in the horizontal plane. Now consider the electron a time later at position B. The electron has traveled one-quarter of an undulator period and now experiences a maximum in the laser electric field. The force on the electron at point B is opposite the direction of the laser electric field at that point and is labeled F_e . The electron will therefore experience a decelerating force. Whether an electron is accelerated or decelerated by the laser electric field depends on the phase of the laser electric field with respect to the electron oscillation. Some electrons are accelerated, while those half a laser wavelength ahead or behind are decelerated. For example, an electron at C would be accelerated. As the accelerated electrons catch up to

those which have been decelerated, they form into bunches at the laser wavelength. In other words, the electron beam becomes axially modulated at the laser wavelength of the FEL radiation. [Ref. 3]

Figure 1-3 [Ref. 4] depicts approximately 10^6 electrons being bunched within the optical wavelength of the FEL radiation while within the undulator.

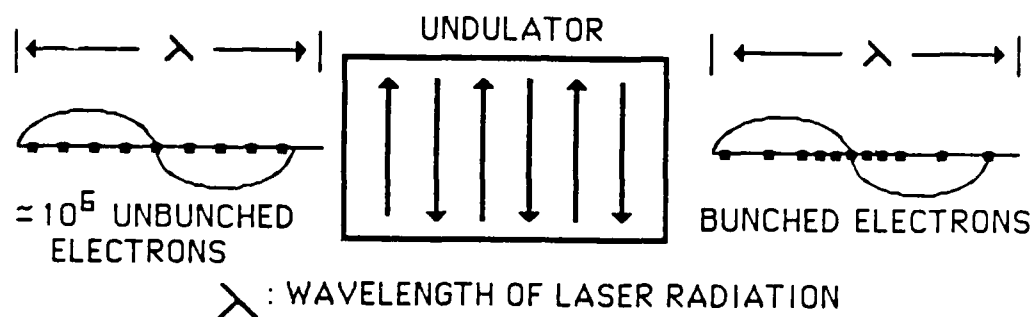


Figure 1-3 Bunching of Electrons within the Wavelength of Laser Radiation

As the electrons oscillate they spontaneously emit "magnetic bremsstrahlung" peaked in the forward direction thus generating the laser electric field. When the laser frequency is nearly resonant with the electron oscillations, significant amounts of energy can be exchanged between the electrons and the laser field causing the bunching effect of the electron beam. The condition for this resonance is given by Equation 1-1 (MKS) [Ref. 5]:

$$\gamma^2 = \lambda_w / 2\lambda (1 + e^2 B_{rms}^2 \lambda_w^2 / 4\pi^2 m_0^2 c^2), \quad (1-1)$$

where:

γ = energy of resonant electron divided by rest mass energy,

λ_w = wiggler (undulator) magnetic period,

λ = laser wavelength (operating wavelength),

e = electron charge,

B_{rms} = rms magnetic induction of the wiggler,

c = velocity of light in vacuo.

The operating (lasing) frequency of a FEL is determined by Equation 1-2 (MKS),

$$\lambda = \lambda_w / 2\gamma^2 (1 + K^2), \quad (1-2)$$

where:

K = the dimensionless measure of the wiggler strength,

$$K = eB_{rms}\lambda_w / 2\pi m_0 c. \quad (1-3)$$

The operating parameters of the Stanford MKIII IRFEL are shown in Table 1-1 [Ref. 6].

The wiggler period of the IRFEL is of the "hybrid" type employing both SmCo permanent magnets and vanadium permendur steel poles. The magnets are oriented to provide a nearly

TABLE 1-1
MKIII IRFEL PARAMETERS

WIGGLER

magnet period	λ_w	2.3	cm
number of periods	N	47.5	
minimum gap	g_{min}	6.5	mm
wiggler strength	K	1.14	
peak magnetic field	B_0	0.702	T

RESONATOR

length	L	178.57	cm
Rayleigh range	z_R	73	cm

E-BEAM

energy	γ	85	
energy	E	43	MeV
energy spread	$\delta\gamma/\gamma$	0.5	%
peak current	I	20	Amps
emittance	ϵ_N	7	π -mm mrad
macropulse length	τ	3	μ sec

sinusoidal vertical field B_y , using a Halbach undulator design. [Ref. 6] The lasing frequency can be modified by slightly changing the energy of the beam or by changing the K value of the wiggler. In practice the K parameter is modified by adjusting the gap between the permanent magnets in the wiggler cavity. The resonator length must then be modified to account for the new wavelength. Assuming the

lasing wavelength of 3.0 microns, the IRFEL will produce a modulated beam as shown in Figure 1-4.

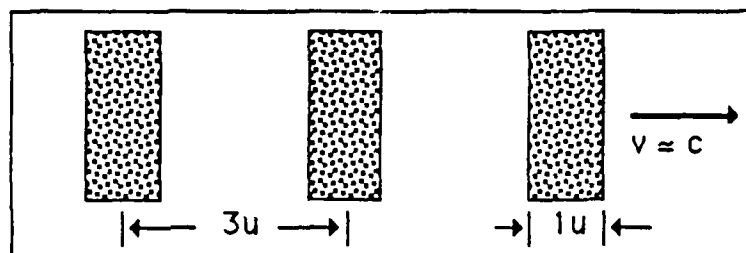


Figure 1-4 Disks of Charge (picobunches)

The rectangles indicate disks of charge of thickness 1 micron separated by 3 microns. This periodic bunched pulse train will generate transition radiation of wavelength 3 microns and also odd harmonics when passing through a thin foil such as mylar or aluminum. The current vs time profile is shown in Figure 1-5.

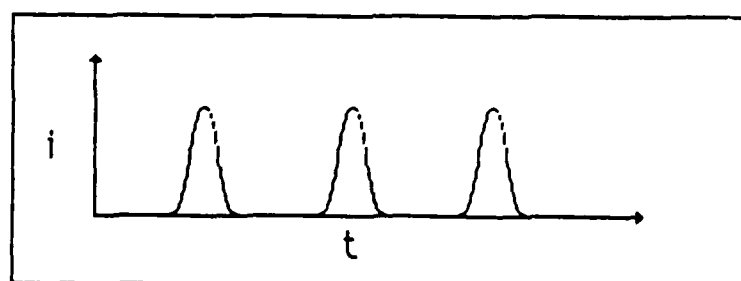


Figure 1-5 Current pulses

C. WHAT IS TRANSITION RADIATION

Transition radiation (TR) is the electromagnetic radiation which is emitted when a uniformly moving charged particle traverses from one medium into another with a different dielectric constant. More generally the effect will occur in the presence of a heterogeneity in a medium. [Ref.7]

TR may be considered to originate from the change in the fields as an electron crosses a boundary. The magnetic field remains essentially constant but the electric field changes because of the change in the dielectric constant. A third field, radiation, is required to meet the boundary conditions.

TR can also be explained in terms of a charge and its image. While an electron moves uniformly in vacuo it does not radiate; the field in vacuo is equal to the field of the electron and its image moving toward it. When the electron crosses the boundary surface both the electron and its image cease to exist from the point of view of the field. The crossing of the boundary must give rise to exactly the same radiation as that which is due to a sudden stop at the same point of the electron and its image. [Ref. 7]

The free electron laser will longitudinally modulate the electron beam in the undulator/wiggler yielding disks of charge of small thickness (1μ). Due to the low efficiency of OTR, 10^6 electrons per picobunch will yield approximately 10^4 photons per picobunch upon foil impact.

For a relativistic beam of electrons ($\beta \rightarrow 1$), and a TR foil inclined at 45 degrees with respect to the beam axis

(Figure 1-1), the backward/specular reflection intensity for a vacuo/dielectric interface is given by the relation [Ref. 2]:

$$d^2I/d\omega d\Omega = F(\psi, \omega) (e^2/\pi^2 c) [e^2/(\gamma^{-2} + \theta^2)^2], \quad (1-4)$$

where:

$$F(\psi, \omega) = \left[\frac{[\epsilon - \sin^2(\psi + \theta)]^{1/2} - \epsilon \cos(\psi + \theta)}{[\epsilon - \sin^2(\psi + \theta)]^{1/2} + \epsilon \cos(\psi + \theta)} \right]^2$$

F = Fresnel coefficient for reflection of light with the E-vector in the plane of incidence,

ψ = angle of specular reflection (45 degrees),

ϵ = dielectric constant of foil material.

The intensity of this radiation should be sufficient for the detection and observance of TR from a single foil/multi-electron interface. Measurement of the radiation will be accomplished via a detector of the phototube, TV camera, or reticon type.

The characteristics of TR that will apply to the proposed experiment are:

- (1) The angular distribution of TR is such that for relativistic particles the emission angle of the photons with respect to the electron beam is approximately equal to $1/\gamma$.
- (2) The intensity of TR is a strong function of the energy of the particle producing it.

- (3) The radiation is polarized with the electric field in the plane containing the particle velocity vector and the wave propagation vector.
- (4) In the case of a periodic medium (i.e., multifoil) an $r\pi$ phase difference is the condition for constructive interference or resonance between radiation produced at successive interfaces; r is a positive integer. For m boundaries the intensity varies as m^2 .
- (5) If the medium is a transparent dielectric then $\epsilon' = n^2(\omega)$, where n is the refractive index and ϵ' is the dielectric constant.
- (6) For a relativistic electron, TR will arise at the surface of the interface. [Ref. 7]
- (7) The power radiated from a transition foil is proportional to the charge squared [Ref. 2].

II. PROPOSED EXPERIMENT USING MKIII IRFEL

A. EXPERIMENT PROPOSAL

The purpose of this experiment will be to measure the electron beam modulation of the FEL using a TR foil.

The MKIII IRFEL, located at the High Energy Physics Lab at Stanford University may lend itself to an experiment to measure the axial modulation of the electron beam of the FEL. The "bunched" beam downstream of the wiggler magnet is normally bent away from the downstream cavity mirror and directed to the beam dump. If the beam were to retain its axial modulation, upon the passage through a thin foil it would generate coherent transition radiation. The thin foil will hereafter be referred to as the detector. The detector must be conveniently located downstream of the wiggler.

1. System Description

The MKIII IRFEL is shown in Figures 2-1, 2-2, 2-3, and 2-4. Figure 2-1 is a photo of the accelerator section of the IRFEL. Figure 2-2 is a representation of the IRFEL downstream of the accelerator. The electron beam produced by the accelerator is directed around the upstream optical cavity mirror and through the wiggler magnet. The beam is axially modulated within the wiggler and is then directed around the downstream movable mirror to the beam dump. An

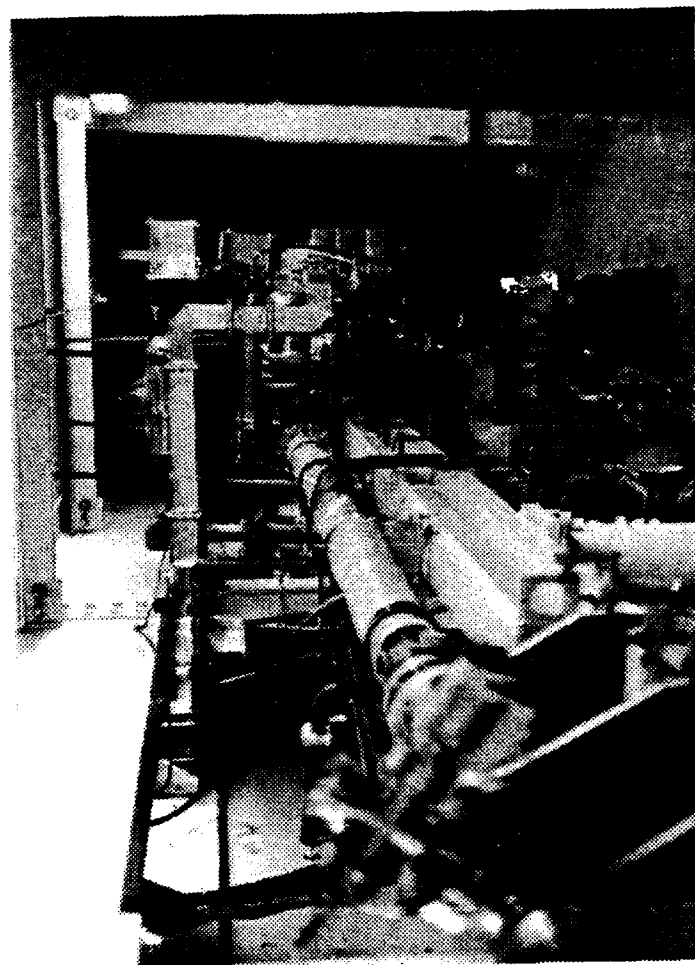


Figure 2-1 MKIII IRFEL Accelerator

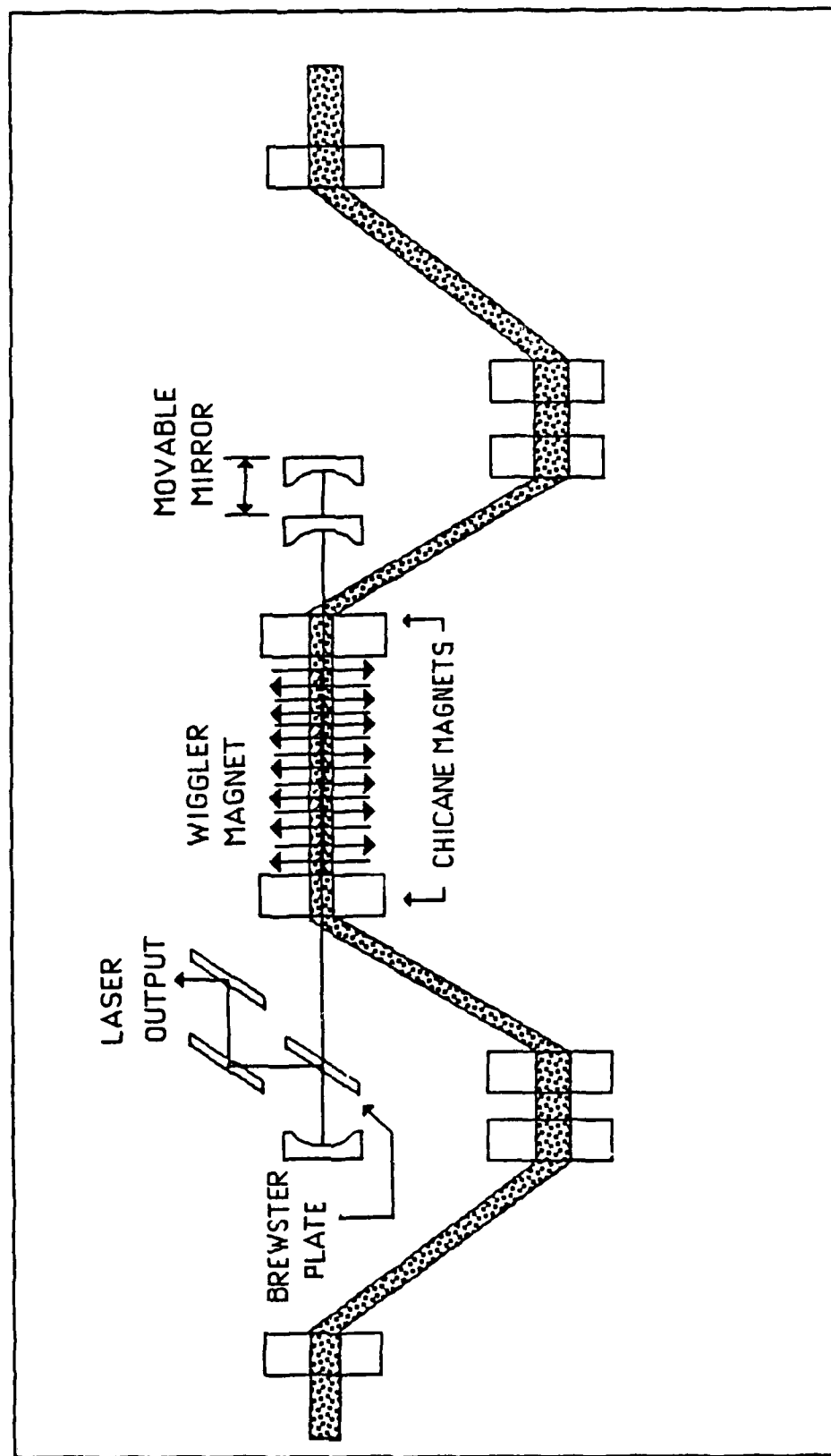


Figure 2-2 MKIII IRFEL

external photo of the MKIII IRFEL wiggler magnet is shown in Figure 2-3.

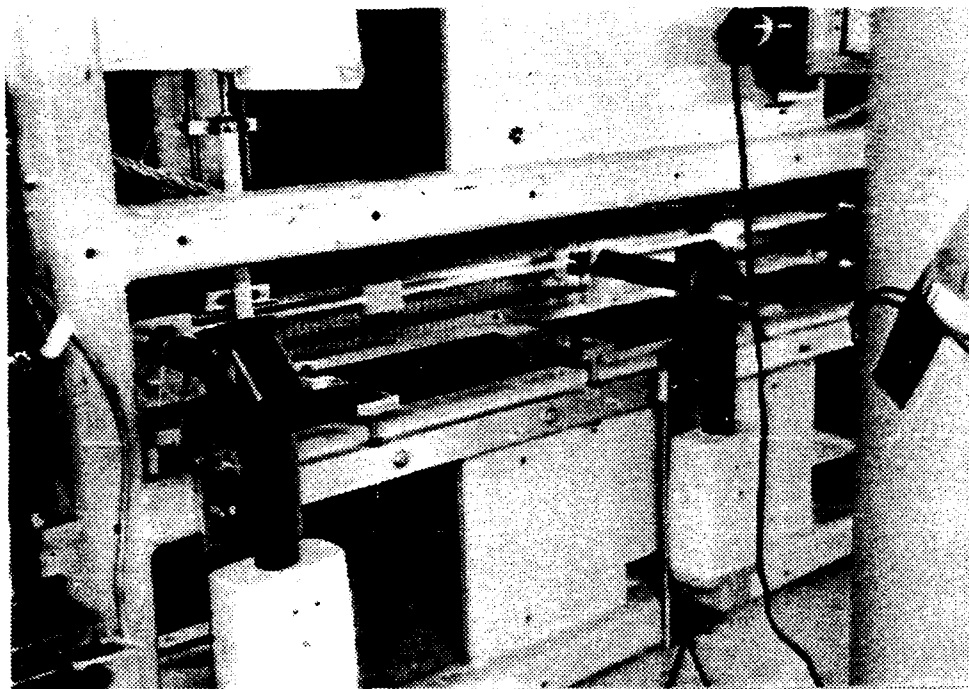


Figure 2-3 MKIII IRFEL Wiggler

Figure 2-4 is a photo of the experimental beamline apparatus downstream of the wiggler cavity. The electron beam will proceed from left to right. The figure shows the waveguide type piping, flanges, bending magnet #2, bending magnet #3, and a four way cross. Bending magnet #1 is upstream to the left of the flange and bellows (not shown in the photo). The detector could easily be placed on the waveguide piping or at the four way cross location.

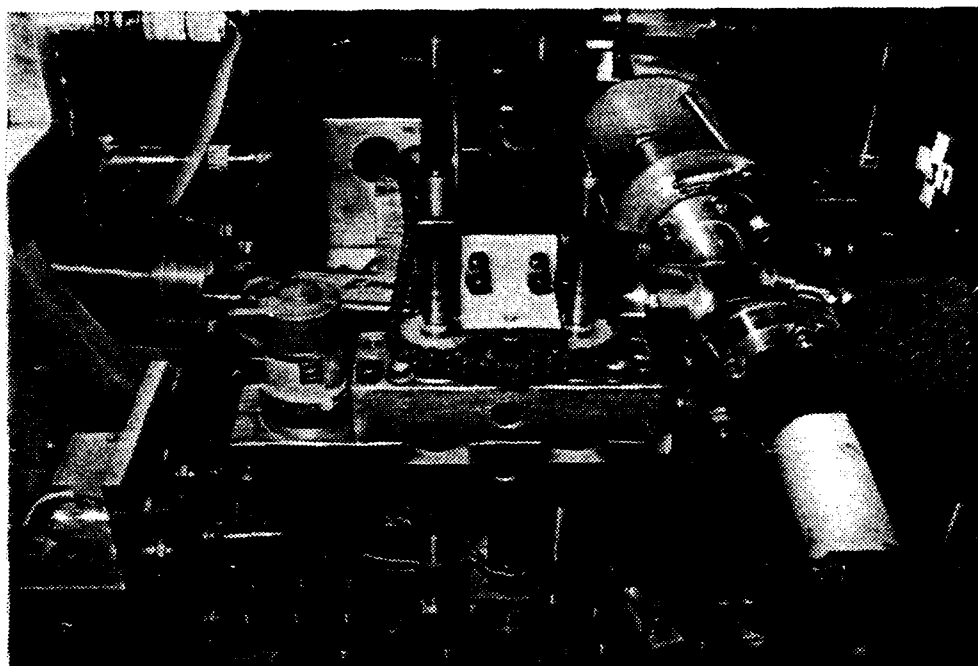


Figure 2-4 MKIII IRFEL Wiggler Exit

2. Possible Detector Locations

Figure 2-5 is a top view representation depicting possible locations for the detector. The electron bunches exiting from the wiggler are deflected by the first bending magnet in order to prevent them from striking the resonator mirror.

3. Hardware Design at Detector Locations

The hardware design needed for a detector between locations B and C is shown in Figure 2-6. Placement of the detector between points B and C would require modifying the waveguide piping, bellows, and flange. Location E is the alternative location of the detector and would require the

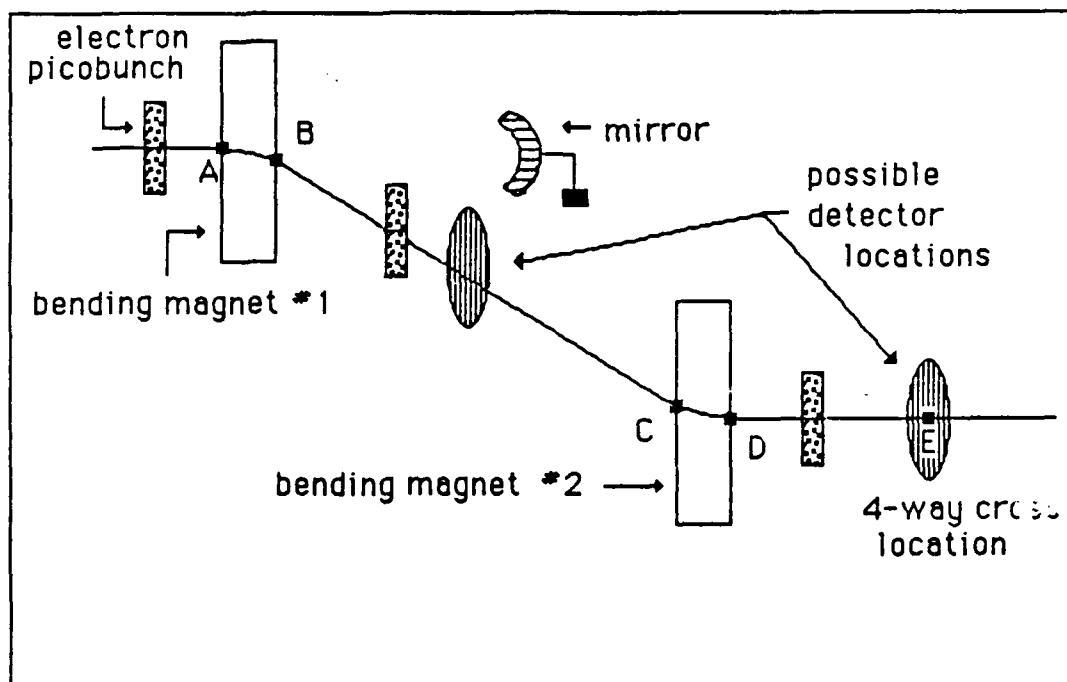


Figure 2-5 Detector Locations

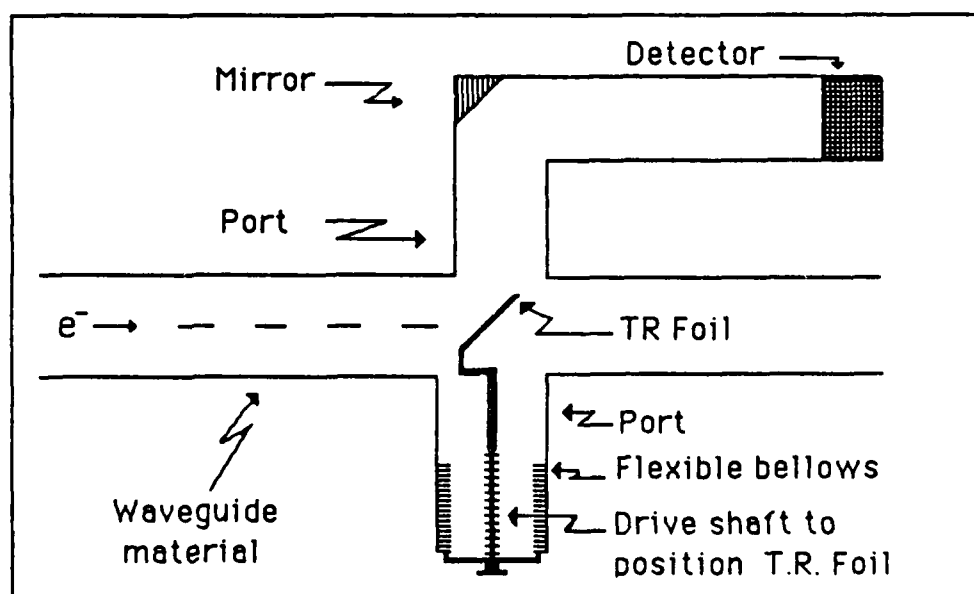


Figure 2-6 Detector Placement on Waveguide

modification of Figure 2-7A. The linear motion feedthrough needs to be connected to a sliding sleeve device in order to position the TR foil and mirror. A suitable sliding sleeve device is shown in Figure 2-7B. In general, it would be easier to modify the IRFEL by placing the detector at location E.

B. ANALYSIS OF ELECTRON BEAM TRANSPORT EQUATIONS

Note: Readers not familiar with the properties of beams and the TRANSPORT development of system equations should read Appendices A and B before proceeding with this section.

The development of the electron beam transport equations for locations A through E along the central trajectory is found in Appendix B. It is desired to find the best location in the beamline to place the detector in order to generate coherent transition radiation. Of particular concern is the longitudinal extent of the picobunches (Figure 1-3) as they traverse the beamline. In the ideal case the picobunches would retain their axial modulation traversing the beamline. This is the case of a non-divergent, monoenergetic beam. In the real world, electron beams are non-monoenergetic and are divergent. Beams of this nature are specified in terms of their phase space. In order to observe coherent transition radiation, the picobunches must not "debunch" significantly upon traversing the beamline. "Significant" debunching for this experiment is on the order of a few (>3) microns. If debunching

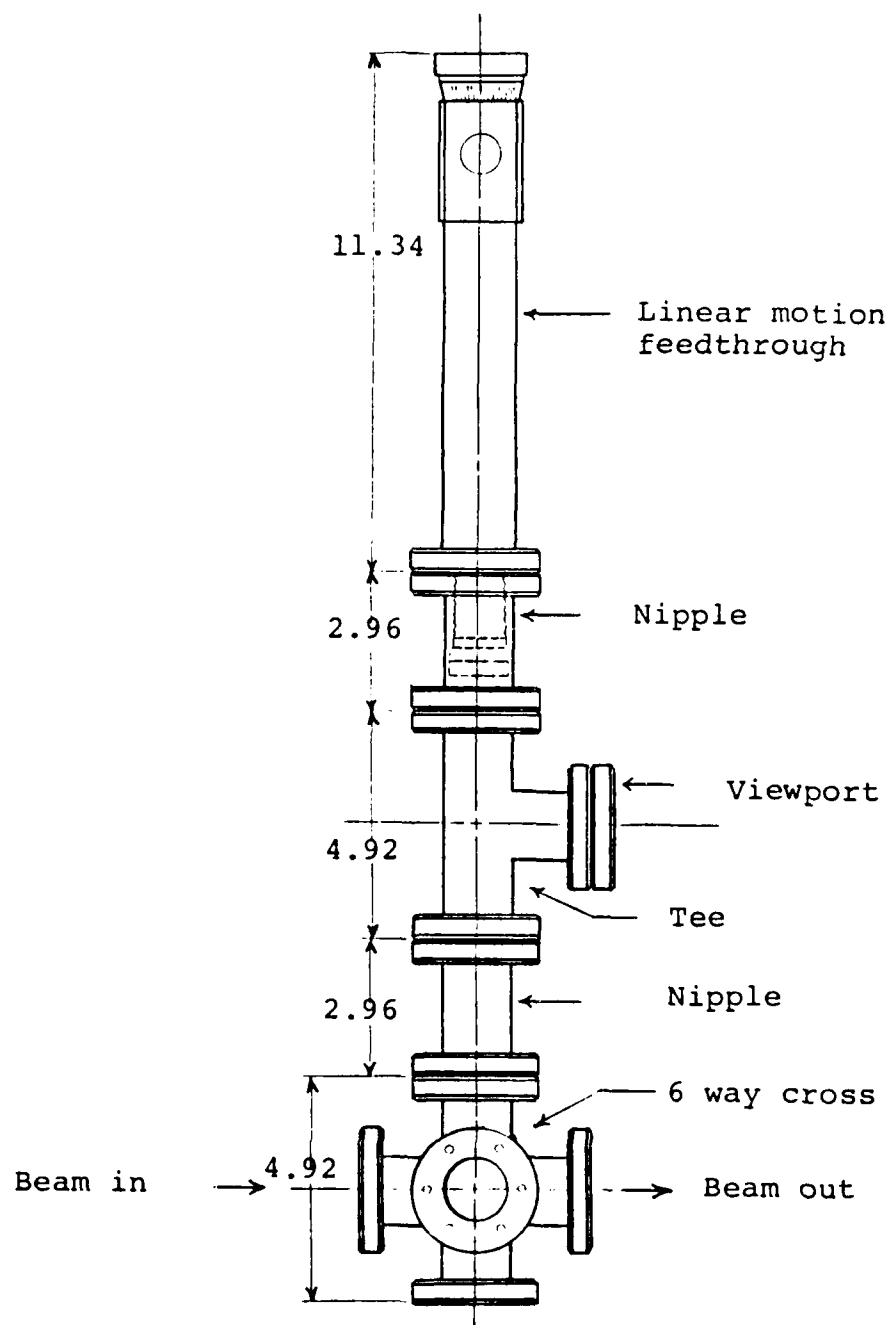


Figure 2-7A Detector Placement at Location E
(All Dimensions in Inches)

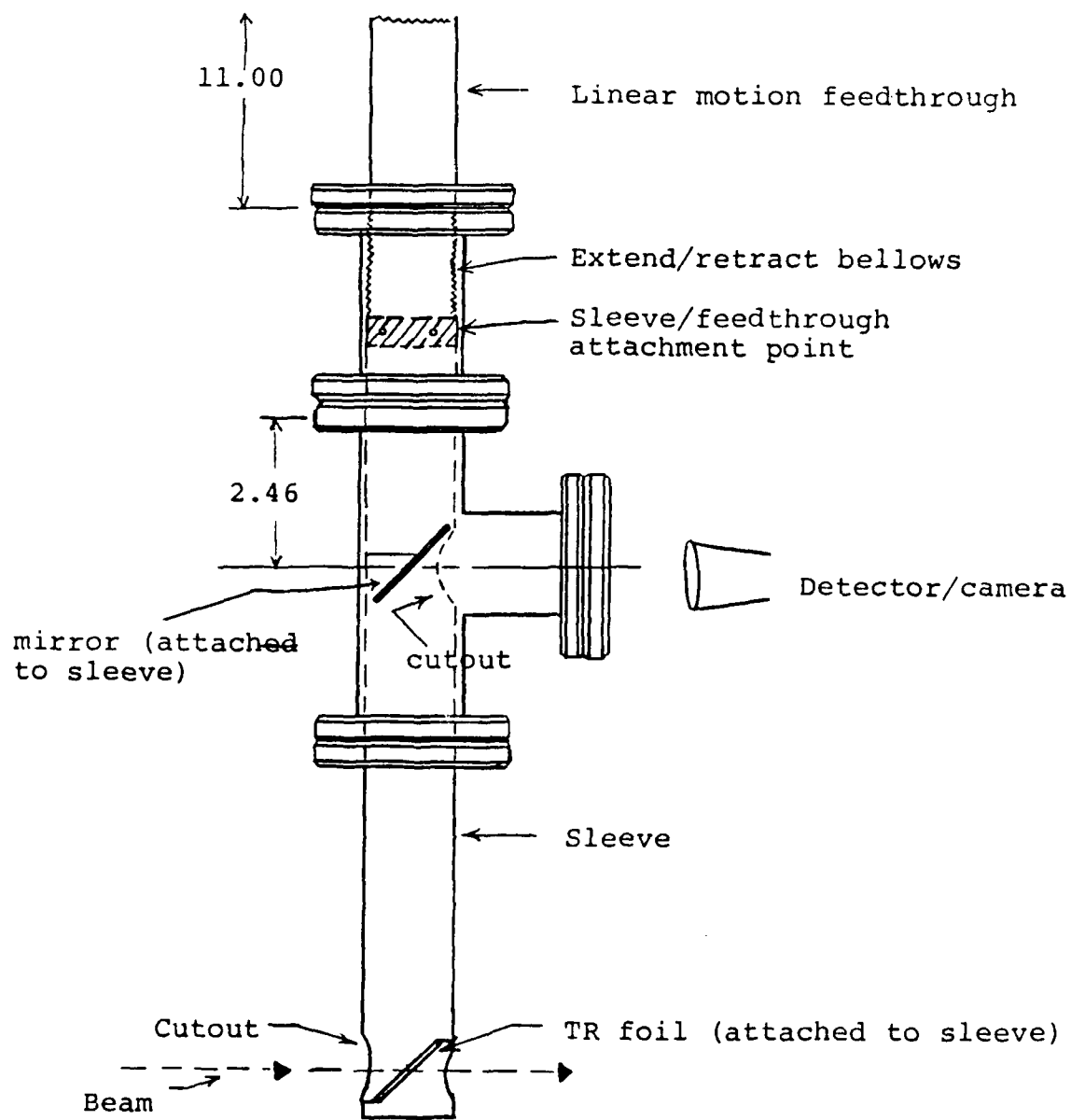


Figure 2-7B Sliding Sleeve Device
(All Dimensions in Inches)

exceeds 3 microns the coherent TR effect will not be observed. A simple representation of the beam traversing the system is desired. Figure 2-8 is a representation of the paths a single electron located at "a" may take in traversing the system. System parameters (obtained from blueprint) and definitions applicable to the representation are shown below the figure.

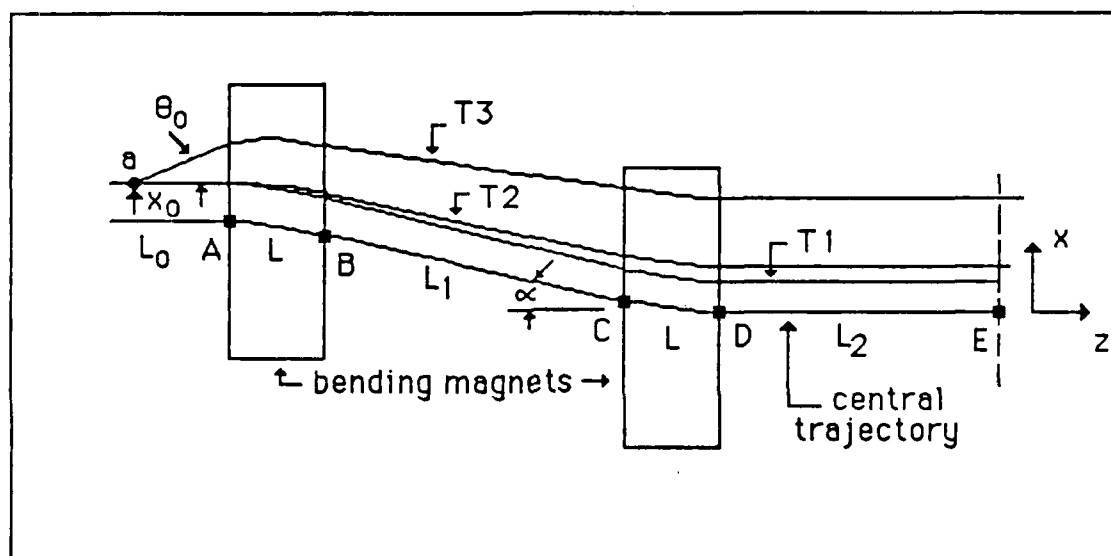


Figure 2-8 Trajectory of a Single Electron

- x_0 = the initial horizontal displacement of the electron with respect to the central trajectory.
- θ_0 = the divergence of the electron with respect to the assumed central trajectory.
- δ_0 = the fractional momentum deviation of the electron from the assumed central trajectory.

The central trajectory parameters are:

L_1 = drift length 1	327.03 mm
L_2 = drift length 2	95.30 mm
L = effective pathlength through bending magnet	38.35 mm
α = bending angle	11.25 °
ρ_0 = bending radius of magnet	195.30 mm
L_0 = initial drift length	0.0 mm
E = energy of electron	40 MeV

(Note: $L_0 = 0$; the electron starts at the magnet pole face)

1. Buskirk System Equations

The system equations for this model were derived by Dr Fred Buskirk. These equations assume the initial drift length, L_0 and the effective pathlength through the bending magnet, L , equal zero. The derived equations are:

$$dx = (L_1/\cos^2\alpha + L_2)\theta_0 + (L_1\sin\alpha/\cos^2\alpha)\delta_0 + x_0, \quad (2-1)$$

$$ds = -(L_1\sin\alpha/\cos^2\alpha)\theta_0 - (L_1\tan^2\alpha)\delta_0, \quad (2-2)$$

where:

dx = the change in the horizontal distance of the electron with respect to the central trajectory, and

ds = the difference in the pathlength between the arbitrary ray and the central trajectory.

The electron is to traverse the system from point "a" to the xy plane of location E. Assuming the fringing fields are negligible the electron will bend in the xz plane only.

Trajectory 1 (T1) is for the case of the monoenergetic ($\delta_0 = 0$) non-divergent ($\theta_0 = 0$) electron initially located at x_0 . Its trajectory coincides with the central trajectory as expected. Trajectory 2 (T2) is the case of a non-monoenergetic non-divergent electron initially located at x_0 . Since this electron possesses greater momentum than the central momentum it will not be bent as much by the bending magnets. The pathlength between the bending magnets will be shorter than L_1 . If two electrons having equal velocities were located at "a" start downstream on trajectories T1 and T2, the electron on T2 would have a shorter pathlength through the system. At the time when the electron on T1 reached the xz plane of location E, the electron on T2 would have already passed through the system by a distance equal to the pathlength difference. T2 is also slightly greater than T1 in the x direction. Trajectory 3 (T3) is the case of a non-monoenergetic, divergent electron initially located at x_0 . As this electron traverses the system on T3, the pathlength between the bending magnets will be different from the central trajectory and the electron would end up at a different location downstream. The three electron trajectories illustrate the change in pathlength due to the effects of

divergence and percent momentum change. This is analogous to the change in the longitudinal extent of a picobunch as it traverses the system.

2. TRANSPORT Equations

The TRANSPORT equations for location E are derived in Appendix B. These equations are:

$$x_E(t) = (2\rho_0 \tan \alpha + L_1 / \cos^2 \alpha + L_2) \theta_0 \\ + (-2\rho_0 + 2\rho_0 / \cos \alpha + L_1 \sin \alpha / \cos^2 \alpha) \delta_0, \quad (M-13)$$

$$l_E(t) = (-2\rho_0 + 2\rho_0 / \cos \alpha + L_1 \sin \alpha / \cos^2 \alpha) \theta_0 \\ + (-2\rho_0 \alpha + 2\rho_0 \tan \alpha + L_1 \tan^2 \alpha) \delta_0 + l_0. \quad (M-15)$$

It can be shown that the TRANSPORT equations reduce to the Buskirk equations letting the effective pathlength through the bending magnet, L , and the initial one-half longitudinal extent of the picobunch, l_0 , equal zero. The variables x and l correspond to dx and ds respectively in Equations 2-1 and 2-2. TRANSPORT analysis requires the phase space representation of the input beam. For a normalized horizontal beam emittance of 8 mm-mrad (revised MKIII IRFEL parameter) with a beam energy of 40 MeV, assume the 2-D phase space of Figure 2-9. The points a-d corresponding to the extreme values of the phase space ellipse are to be plotted. This will yield a physical representation of what the detector will see at the location of interest.

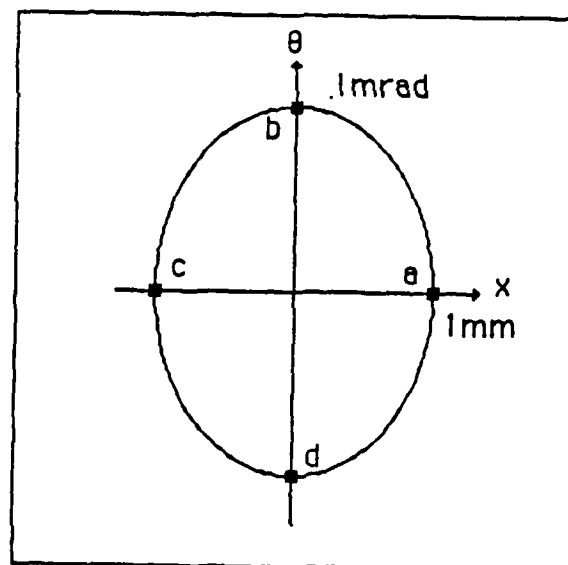


Figure 2-9 2-D Phase Space

Substituting the system parameters with $l_0 = .0005$, Equations M-13 and M-15 become:

$$x(t) = .51296\theta_0 + .73976\delta_0 + x_0, \quad (2-3)$$

$$l(t) = .07398\theta_0 + .13940\delta_0 + .0005, \quad (2-4)$$

where x_0 , $x(t)$, l_0 , $l(t)$ are in mm; θ_0 in mrad, δ_0 in $\% \Delta P/P$. The plot of $x(t)$ vs $l(t)$ for the points in Figure 2-9 is shown in Figure 2-10. Tabulated values are shown in Table 2-2. The center ellipse corresponds to a mono-energetic picobunch with divergence in the xz plane. The divergence alone causes a significant increase in the picobunch extent. A picobunch of longitudinal extent 1 micron grows to a longitudinal extent of approximately 14

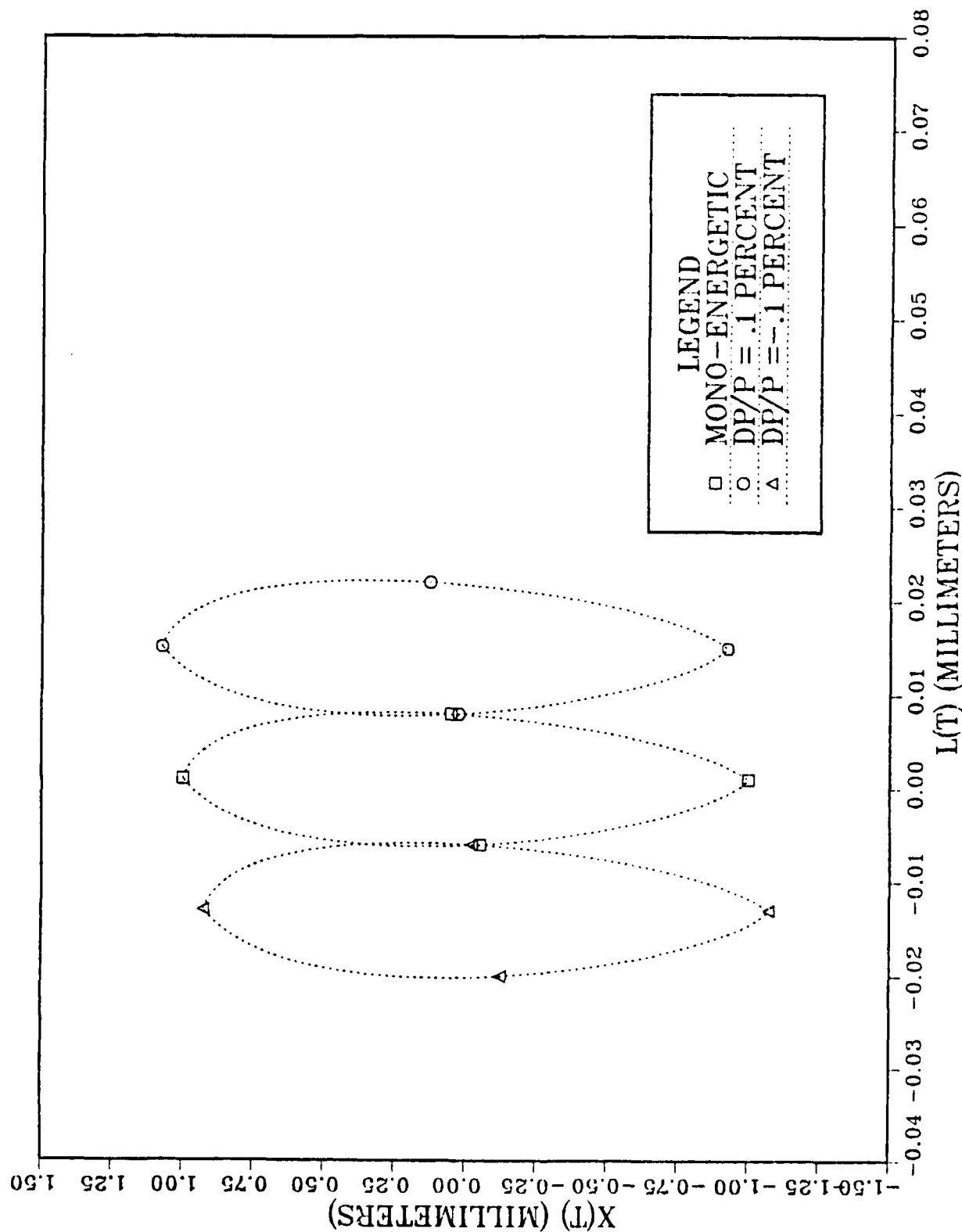


Figure 2-10 Picobunch Extent at Location E

microns at location E. The right side ellipse represents the same picobunch having one-tenth of one-percent greater momentum and the left side ellipse represents the picobunch with one-tenth of one-percent less momentum. A non-monoenergetic picobunch with $\delta_0 = \pm .1\%$ (revised MKIII IRFEL parameter) would have a total longitudinal extent of ≈ 46 microns at location E. A coherent TR effect would not be expected under these conditions. Even in the monoenergetic case, the beam divergence would have to be greatly reduced to yield a longitudinal extent of ≤ 3 microns. The TRANSPORT system equations for detector placement midway between locations B and C are:

$$x_C(t) = (\cos\alpha)x_0 + (\rho_0\sin\alpha + L_1/\cos\alpha)\theta_0 + [\rho_0(1-\cos\alpha) + L_1\tan\alpha]\delta_0, \quad (M-5)$$

$$l_C(t) = (-\sin\alpha)x_0 - \rho_0(1-\cos\alpha)\theta_0 + l_0 - \rho_0(\alpha-\sin\alpha)\delta_0. \quad (M-7)$$

Substituting the known parameters with $L_1 = 163.52$ mm these equations become:

$$x(t) = .98079x_0 + .20482\theta_0 + .36278\delta_0, \quad (2-5)$$

$$l(t) = -.19509x_0 - .00375\theta_0 - .00246\delta_0 + .0005. \quad (2-6)$$

A plot of $l(t)$ vs $x(t)$ for the phase space of Figure 2-9 is shown in Figure 2-11. Tabulated values are shown in Table 2-3.

Inspection of Figure 2-11 reveals a shift in the orientation of the ellipses with respect to Figure 2-10. An 11.25 degree rotation of the thin foil about the y-axis will minimize the total longitudinal extent of the original picobunch as seen by the thin foil. The effective longitudinal extent of the original picobunch is approximately 23 microns for constant $x(t)$. Moving the detector further upstream to a location 10 mm downstream of the first bending magnet the TRANSPORT system equations are:

$$x(t) = .98079x_0 + .04830\theta_0 + .05742\delta_0, \quad (2-7)$$

$$l(t) = -.19509x_0 - .00375\theta_0 - .00246\delta_0 + .0005. \quad (2-8)$$

A plot of $l(t)$ vs $x(t)$ for this detector location is shown in Figure 2-12. Tabulated values are shown in Table 2-4. Note that Equation 2-6 and Equation 2-8 are identical, thus the longitudinal extent of the picobunch is constant between B and C. However, the effective picobunch extent will increase between B and C. Figure 2-12 reveals that a momentum spread of one-tenth of one-percent will not cause significant increase in the effective longitudinal extent of

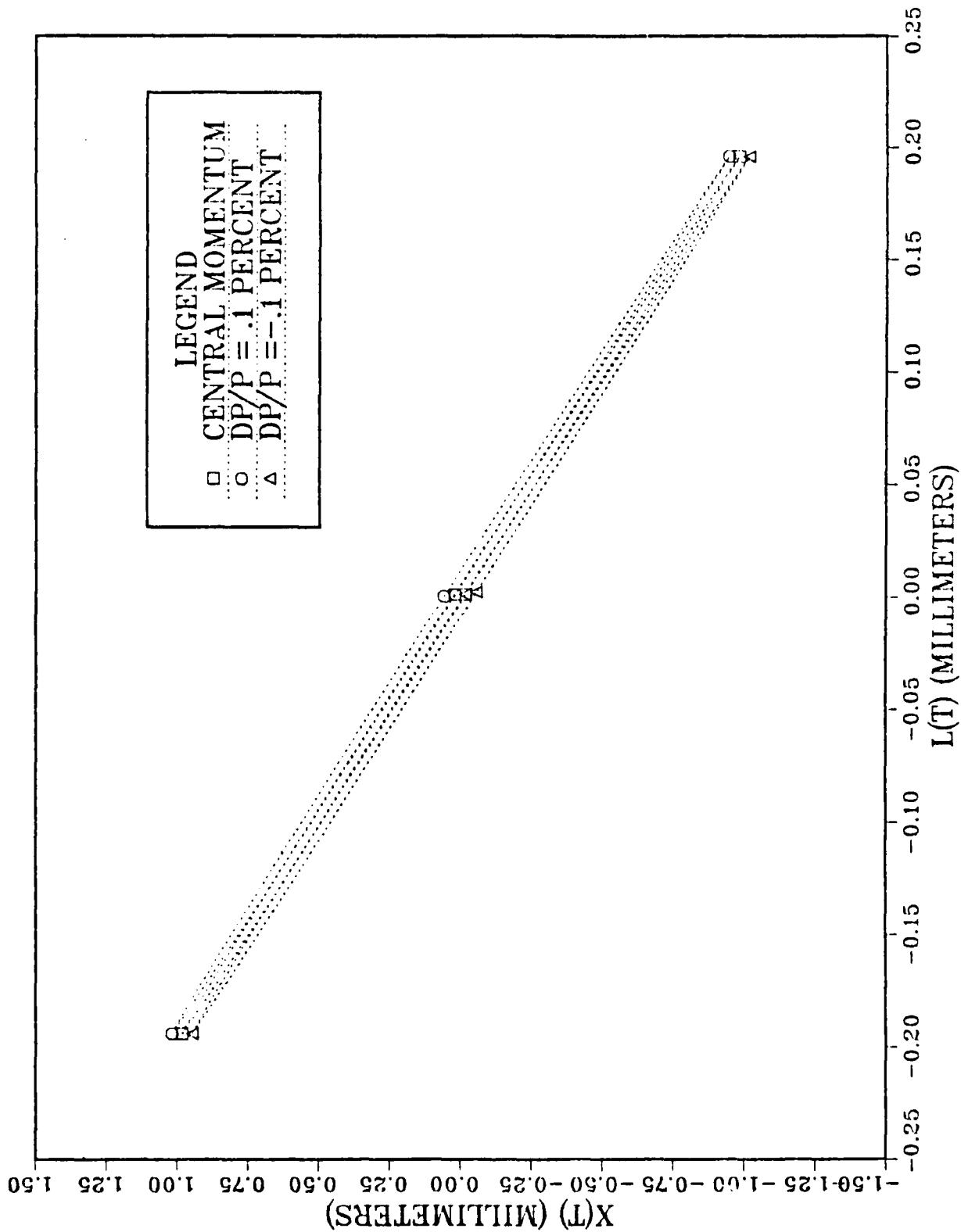


Figure 2-11 Picobunch Extent Halfway Between Bending Magnets

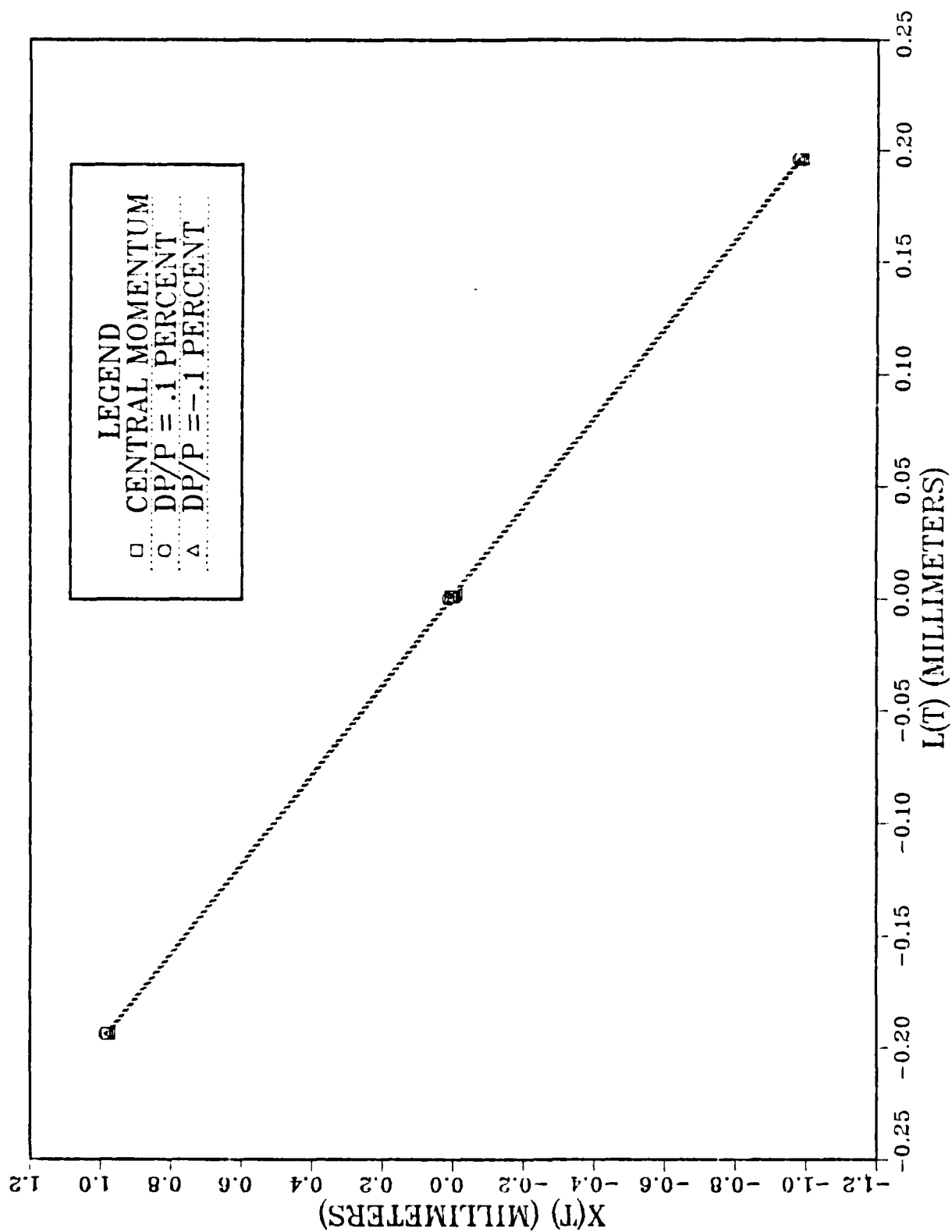


Figure 2-12 Picobunch Extent at 10 mm

the picobunch. The non-monoenergetic ellipses appear to closely coincide with the central momentum ellipse.

It is apparent from equations M-7 and M-15 that the change in the longitudinal extent of the original picobunch is due to the initial horizontal displacement of the electron, x_0 , the divergence of the electron, θ_0 , and the momentum increment, δ_0 ; all with respect to the assumed central trajectory. A scaled plot is used to illustrate the relative effect of each factor contributing to the change in the horizontal and longitudinal extent of the picobunch as it traverses the system. Substituting the known parameters, the TRANSPORT equations to be plotted reduce to the equations of Table 2-1.

TABLE 2-1
EQUATIONS FOR TRAJECTORY PARAMETERS
AT VARIOUS LOCATIONS

Detector 10 mm from bending magnet #1:

$$x(t) = .98079x_0 + .04830\theta_0 + .05742\delta_0$$

$$l(t) = -.19509x_0 - .00375\theta_0 + l_0 - .00246\delta_0$$

Detector halfway between bending magnets #1 and #2:

$$x(t) = .98079x_0 + .20482\theta_0 + .36278\delta_0$$

$$l(t) = -.19509x_0 - .00375\theta_0 + l_0 - .00246\delta_0$$

Detector at location E:

$$x(t) = x_0 + .51296\theta_0 + .73976\delta_0$$

$$l(t) = .07398\theta_0 + l_0 + .13940\delta_0$$

Figure 2-13 is an unscaled representation of the effect of the initial horizontal displacement, x_0 , on the longitudinal extent of the beam. The beam parameters are specified by the given 2-D phase space. Figure 2-13 illustrates that the initial horizontal displacement with respect to the central trajectory will have an effect on the longitudinal extent of the beam between the magnets but will have no effect beyond the second magnet at location E.

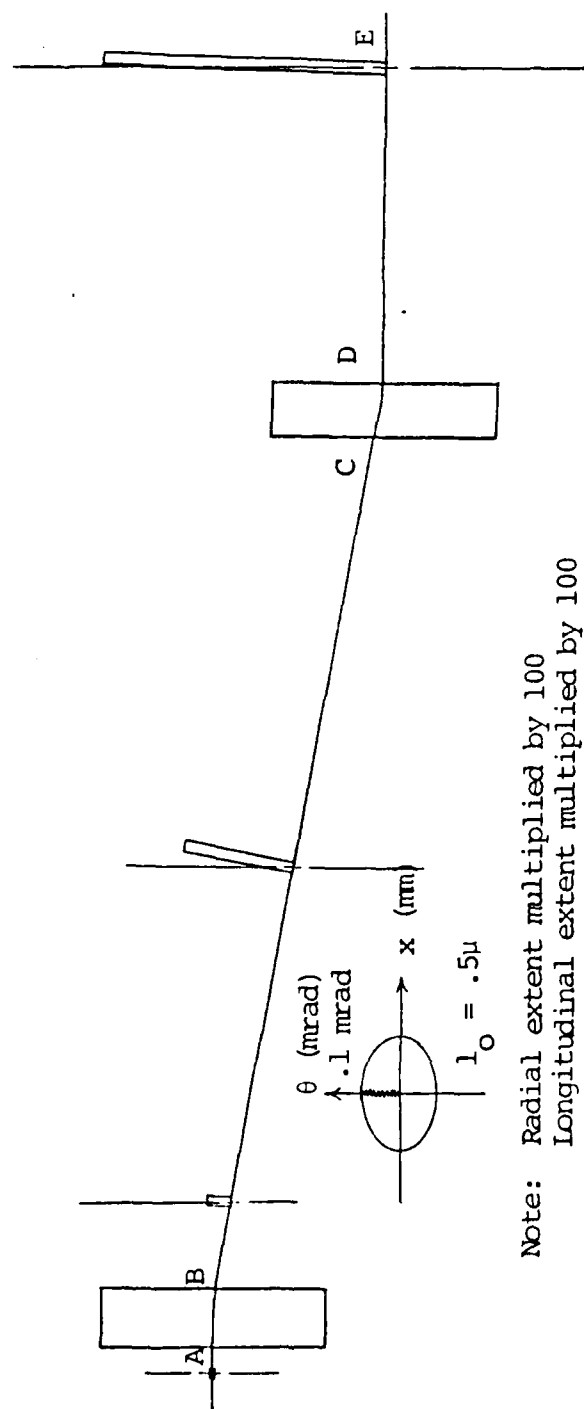
Figure 2-14 is a scaled representation of the effect of the divergence, θ_0 on $x(t)$ and $l(t)$. The effect of the divergence term on $l(t)$ is small over the regions between the magnets but increases beyond the second bending magnet. Note that the change in the longitudinal extent is measured with respect to the beam direction.

Figure 2-15 illustrates the effect of the momentum increment, δ_0 , on $x(t)$ and $l(t)$.

Comparing Figures 2-14 and 2-15, it appears that the divergence and momentum increment have roughly the same effect in debunching the beam picobunches as they traverse the system. The previous three figures and Figures 2-10, 2-11, and 2-12 lead to the physical representation of the beam picobunches shown in Figure 2-16.

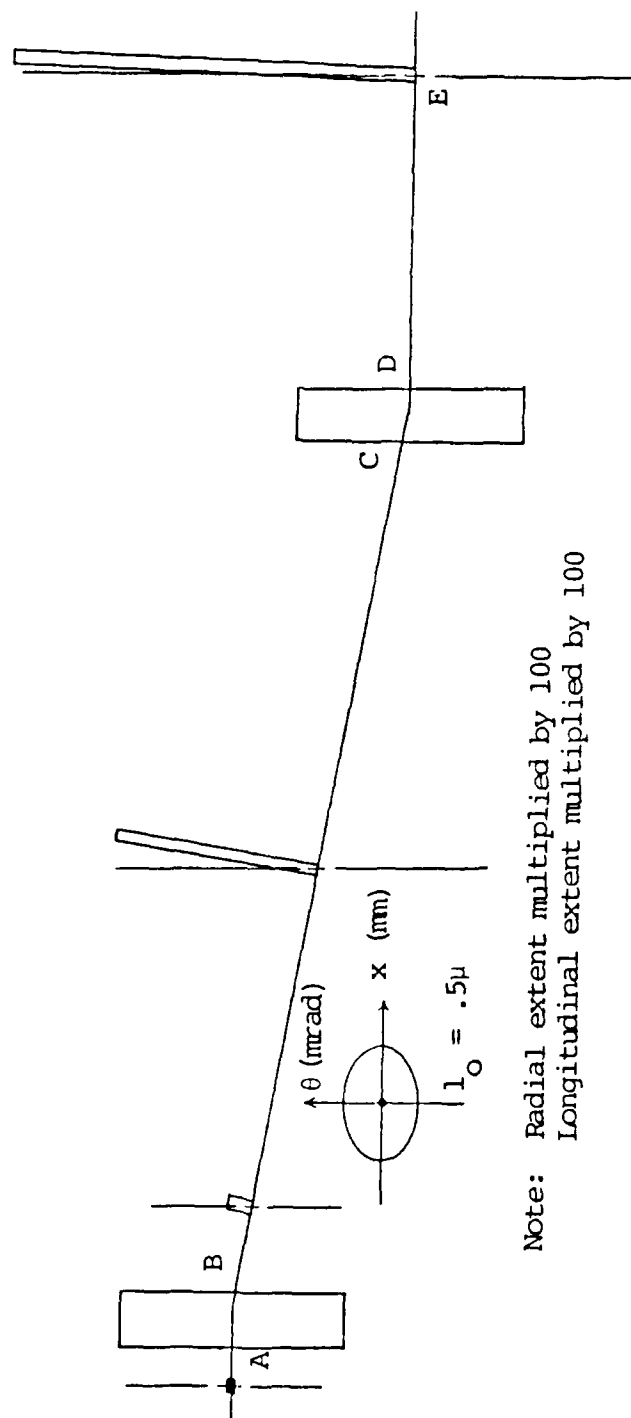


Figure 2-13 Effect of x_0 on $x(t)$ and $l(t)$



Note: Radial extent multiplied by 100
Longitudinal extent multiplied by 100

Figure 2-14 Effect of θ_0 on $x(t)$ and $l(t)$



Note: Radial extent multiplied by 100
Longitudinal extent multiplied by 100

Figure 2-15 Effect of δ_0 on $x(t)$ and $l(t)$

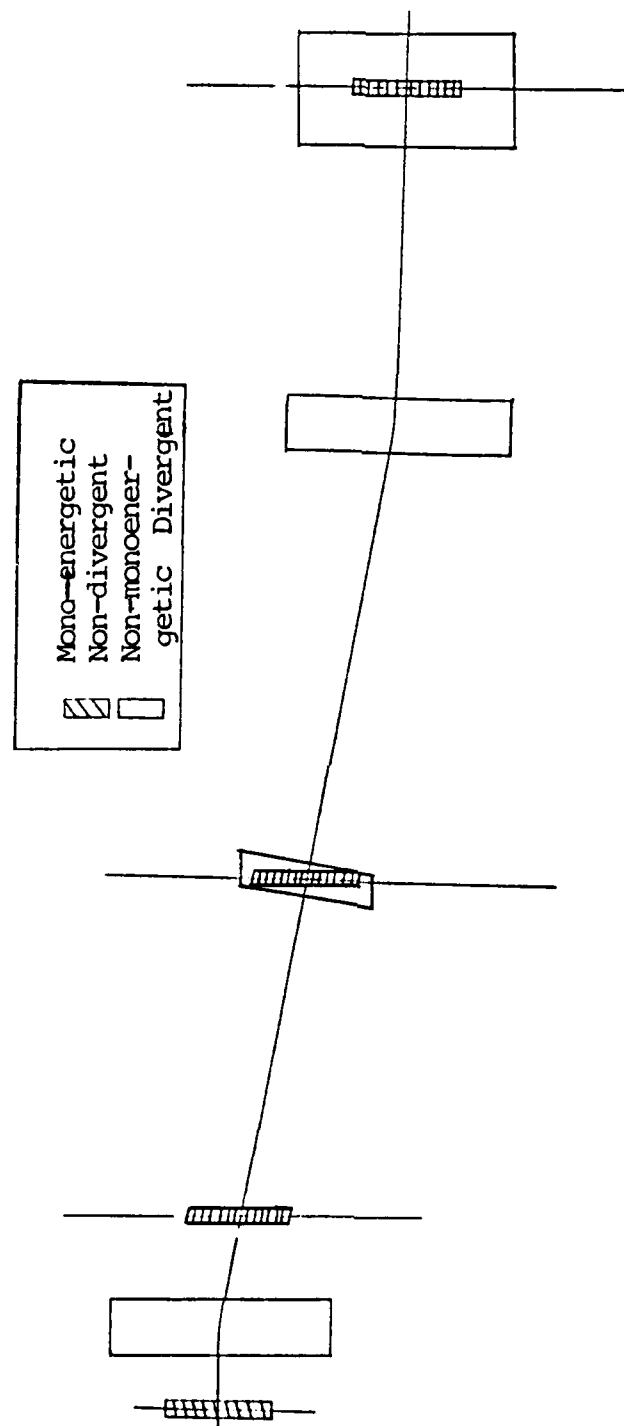


Figure 2-16 Physical Representation of Beam Picobunch

TABLE 2-2

BEAM PARAMETERS FOR DETECTOR AT LOCATION E

<u>Point</u>	<u>(x, θ)</u>	<u>%$\Delta P/P$</u>	<u>l(t) mm</u>	<u>x(t) mm</u>
a	(1,0)	0	.001	1.000
		.1	.015	1.074
		-.1	-.013	.926
b	(0,.1)	0	.008	.051
		.1	.022	.125
		-.1	-.006	-.023
c	(-1,0)	0	.001	-1.000
		.1	.015	-.926
		-.1	-.013	-1.074
d	(0,-.1)	0	-.006	-.051
		.1	.008	.023
		-.1	-.020	-.125

TABLE 2-3

BEAM PARAMETERS FOR DETECTOR HALFWAY
BETWEEN BENDING MAGNETS

<u>Point</u>	<u>(x, θ)</u>	<u>%$\Delta P/P$</u>	<u>l(t) mm</u>	<u>x(t) mm</u>
a	(1,0)	0	-.194	.981
		.1	-.194	1.017
		-.1	-.194	.945
b	(0,.1)	0	.001	.020
		.1	0	.057
		-.1	.001	-.016
c	(-1,0)	0	.196	-.981
		.1	.196	-.945
		-.1	.196	-1.017
d	(0,-.1)	0	.001	-.020
		.1	.001	.016
		-.1	.002	-.057

TABLE 2-4

BEAM PARAMETERS FOR DETECTOR 10 mm
DOWNSTREAM OF FIRST BENDING MAGNET

<u>Point</u>	<u>(x, θ)</u>	<u>%$\Delta P/P$</u>	<u>l(t) mm</u>	<u>x(t) mm</u>
a	(1, 0)	0	-.194	.981
		.1	-.194	.987
		-.1	-.194	.975
b	(0, .1)	0	.001	.005
		.1	0	.011
		-.1	.001	-.001
c	(-1, 0)	0	.196	-.981
		.1	.196	-.975
		-.1	.196	-.987
d	(0, -.1)	0	.001	-.005
		.1	.001	.001
		-.1	.002	-.011

III. RESULTS AND CONCLUSIONS

The axially modulated beam of the MKIII IRFEL was represented as disks of charge (picobunches) as shown in Figure 1-4. If these picobunches were to retain their axial modulation and pass through a thin foil, coherent optical transition radiation would be generated.

The analysis of the TRANSPORT system equations for the detector locations of Figure 2-5 reveal that significant debunching (of more than 3 microns in the axial direction) will occur at these detector locations due to the effects of a non-monoenergetic, divergent beam.

For detector placement at the four-way cross location (location E of Figure 2-5) the increase in the picobunch extent is approximately 46 microns (Figure 2-10). For the detector location halfway between bending magnets #1 and #2 (Figure 2-5) the effective picobunch extent is reduced to 23 microns (Figure 2-11) with the detector rotated 11.25 degrees about the y-axis. Placing the detector further upstream has the overall effect of reducing the effective picobunch extent. The axial modulation of the electron beam of the MKIII IRFEL can be measured at a detector location 10 millimeters downstream of the first bending magnet with the detector rotated 11.25 degrees about the y-axis. At this location there will be a 2 micron increase in the effective

picobunch extent (Figure 2-12). In theory, detector placement at this location will enable the desired OTR effect to be observed. This location, however, is not easily accessible due to structural hardware upstream of the bellows of Figure 2-4. In addition, the bellows location and waveguide material would have to be modified in order to mount a detector of the type illustrated in Figure 2-6. To situate a detector at this location it will be necessary to make hardware modifications to accomodate the experimental arrangement.

The normalized horizontal and vertical emittance parameters for this experimental proposal were 8 mm-mrad and 4mm-mrad respectively. The momentum spread was one-tenth of one percent. A reduction in these parameters will yield a reduced picobunch extent at any detector location.

In addition to the Stanford MKIII IRFEL, there are several IRFELS that are potentially suitable for an experiment of this nature. Potential candidates for this experiment include:

- (1) The Free Electron Laser Driven by the NBS Microtron
- (2) Stanford Superconducting Accelerator/Free Electron Laser SCA/FEL
- (3) Lawrence Livermore National Laboratory ATA/TRW Wiggler.

The NBS CW Microtron Driven FEL (currently under development) has the design goals of a normalized transverse emittance less than 10 mm-mrad and a momentum spread of less

than .03% for operation at 0.2-3.0 microns. This momentum spread is one order of magnitude better than the MKIII IRFEL due to the inherent acceleration process of a microtron. The hardware and bending magnet configuration downstream of the wiggler exit need to be investigated and modeled in order to determine a suitable detector location to measure the electron beam modulation.

The Stanford Superconducting Accelerator/Free Electron Laser (SCA/FEL) has a normalized transverse emittance of 5 mm-mrad (10 mm-mrad with a high brightness injector) and a momentum spread of approximately .04% for a fundamental wavelength of 3u. [Ref.8] The hardware and bending magnet configuration downstream of the wiggler exit also need to be investigated and modeled in order to determine suitability for a proposed experiment.

The Advanced Test Accelerator/TRW Wiggler FEL utilizes induction linac technology and the laser amplifier FEL configuration to amplify a carbon-dioxide laser at 10.6 microns. This system may be more suitable for detector placement due to the absence of optical cavity mirrors and a portable beam dump.

The TRANSPORT equations were generated using a first order approximation and an assumed beam spot size of radius 1 mm at the entrance pole face of the first bending magnet. The accuracy of the equations could be improved by utilizing the second order fitting capability of TRANSPORT.

The system of Figure B-3 was modeled starting at location A, assuming a beam spot size of radius 1 mm. A more accurate model would incorporate the effects on the electron beam envelope within the wiggler. TRANSPORT does not have a designated "wiggler" element however, the wiggler can be modeled using drift spaces and the "Arbitrary Transformation" (type code 14) input option. This model should start at the wiggler center where the beam waists x_w and y_w are known. [Ref. 10]

APPENDIX A

BEAM TRANSPORT THEORY

1. PHASE SPACE

The transport of a charged particle beam through a system of magnets and drift spaces involves the study of a fundamental conservation law known as Liouville's theorem:

. . . under the action of forces which can be derived from the Hamiltonian, the motion of a group of particles is such that the local density of the representative points in the phase space remains everywhere constant. [Ref. 11]

Liouville's theorem advises the reader that he must look at the collective group of particles rather than an individual particle in order to access the overall nature of beam transport. A single particle moving in a three dimensional coordinate system is completely specified if its position and momentum components are known, namely x, y, z, P_x, P_y, P_z . It is convenient to express this information in a six-dimensional space referred to as phase space. A beam comprises all individual particles within this phase space, neglecting electrostatic repulsion and spin dependent effects. The latter two effects would require an unmanageable phase space of dimension six times the number of particles in the beam plus the additional dimensions corresponding to the rotational degrees of freedom of the individual particles. Any system of conservative forces acting on a beam possesses a Hamiltonian. The macroscopic

magnetic forces along the beam trajectory of the proposed experiment are conservative thus the beam must obey Liouville's theorem. The concept of a six-dimensional phase space is a valid and useful utility in the study of beam transport since space charge effects become weaker as beam energy increase. The six-dimensional phase space representing all particles in the beam is considered a hypervolume that can change shape but must maintain constant volume. The phase space analysis of the beam can be further simplified by the choice of the coordinate axis. If the three components of motion are mutually independent in real space, the motion is confined to the three planes (x, P_x) , (y, P_y) , and (z, P_z) . The six dimensional phase space hypervolume has in effect been reduced to three two-dimensional phase space areas. A further simplification in the analysis is possible by assuming the axial momentum of the beam is constant. This is a valid assumption downstream of the accelerator sections of the beam trajectory. The angular divergence of a particle relative to the beam axis is equal to the ratio of the transverse and axial momenta. Considering the transverse x-direction the axial divergence would be P_x/P_z or dx/dz . Dimensional phase space (x, P_x) is now represented as $(x, dx/dz)$ where dx/dz is the angular divergence, a directly observable quantity. Similarly, the transverse y-direction phase space representation is $(y, dy/dz)$. The longitudinal phase space is represented as

($l, dP_z/P_z$) where l denotes the longitudinal beam extent and dP_z/P_z denotes the fractional momentum spread. [Ref. 11]

2. EMITTANCE

The quality of any electron beam is measured in terms of its emittance. Consider a single electron propagating in the z -direction as shown in Figure A-1.

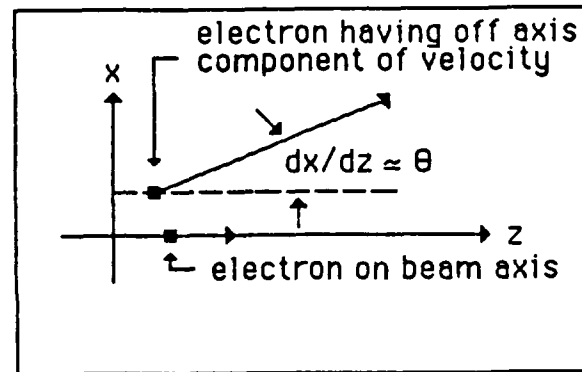


Figure A-1 Single Electron Motion in the Horizontal Plane

Emittance is conveniently expressed in terms of the phase space parameters x and dx/dz . Using the small angle approximation dx/dz can be represented as θ . Electron beams produced by accelerators have elliptical phase spaces as shown in Figure A-2 where:

θ_{\max} = the maximum divergence of an individual electron

x_{\max} = the maximum horizontal extent of a beam electron.

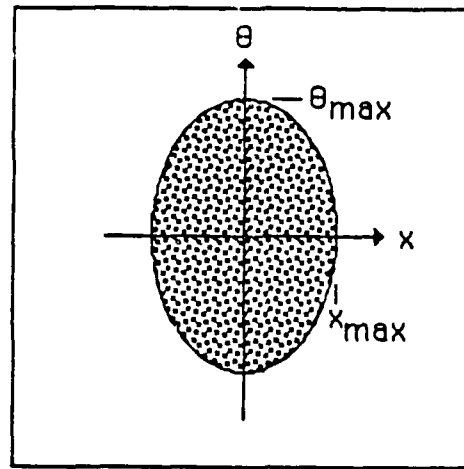


Figure A-2 Elliptical Phase Space

In accordance with Liouville's theorem, phase space is conserved. The electrons are within the perimeter of the ellipse. Emittance is mathematically defined:

$$\epsilon = (\text{area of phase space})/\pi . \quad (\text{A-1})$$

Normalized emittance is defined:

$$\epsilon_n = \beta\gamma\epsilon , \quad (\text{A-2})$$

where γ is the ratio of the particle energy to the rest mass energy and $\beta \approx 1$. The area of the elliptical phase space is $\pi x_{\text{max}}\theta_{\text{max}}$ therefore:

$$\epsilon_h = X_{\max} \theta_{\max}.$$

For example: The Stanford MKIII FEL has the following normalized parameters [Ref. 12]:

horizontal phase space area $\approx 8 \pi \text{ mm-mrad}$,

vertical phase space area $= 4 \pi \text{ mm-mrad}$.

therefore assuming $E = 40 \text{ MeV}$:

$$\epsilon_{nh} = 8 \text{ mm-mrad}; \quad \epsilon_h = .10 \text{ mm-mrad} ,$$

$$\epsilon_{nv} = 4 \text{ mm-mrad}; \quad \epsilon_v = .05 \text{ mm-mrad} .$$

Assuming elliptical phase spaces, we can assign approximate values for X_{\max} and Y_{\max} and the corresponding values for θ_{\max} and ϕ_{\max} .

Letting $X_{\max} = Y_{\max} = 1 \text{ mm}$ and energy equal to 40 MeV with $\beta \approx 1$ the corresponding values of θ_{\max} and ϕ_{\max} are determined to be:

$$X_{\max} = 1 \text{ mm}; \quad \theta_{\max} = .10 \text{ mrad} ,$$

$$Y_{\max} = 1 \text{ mm}; \quad \phi_{\max} = .05 \text{ mrad} .$$

3. BEAM WAISTS

In accordance with electron beam transport design [Ref. 10], the electron beam is normally focussed at the center of the wiggler of the FEL. This yields a beam waist in the center of the wiggler as shown in Figure A-3.

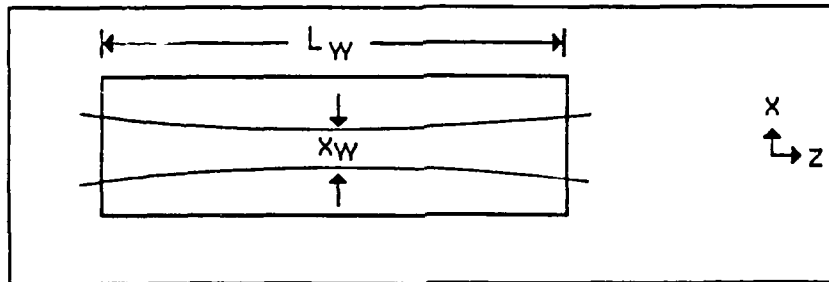


Figure A-3 Beam Focus at Center of Wiggler

where

x_W = horizontal beam waist

y_W = vertical beam waist

L_W = length of wiggler (1 meter)

The horizontal beam waist size is related to the length of the wiggler and the horizontal emittance by the relation:

$$x_W = L_W \epsilon_h / 2 \quad (A-3)$$

The vertical beam waist size is related to the vertical emittance and the intrinsic betafunction, β_w , by the relation:

$$Y_w = \sqrt{\epsilon_v \beta_w} \quad (A-4)$$

where

β_w = electron radius of curvature at center of wiggler.

APPENDIX B

TRANSPORT-A COMPUTER PROGRAM FOR DESIGNING CHARGED PARTICLE BEAM SYSTEMS

1. INTRODUCTION TO TRANSPORT

The study of static-magnetic beam transport systems led to the development of the original first-order TRANSPORT computer program. TRANSPORT was written in BALGOL at Stanford Linear Accelerator Center (SLAC) in 1963. It has been refined in the succeeding years by contributions from various laboratories throughout the world. Subsequent improvements include the translation into FORTRAN and a second-order fitting capability. The version of TRANSPORT used in this thesis is the PC version dated May, 1985 from D. Carey, Fermi National Accelerator Laboratory (FNAL), compiled with the IBM version of professional fortran by Ryan-McFarland. [Ref. 13]

TRANSPORT utilizes matrix theory methods to step sequentially through a beam line system consisting of magnets, drift spaces, and special magnet configurations. The beam line system and the input beam parameters are specified by the user and an output beam matrix and overall system transfer matrix are generated. Each individual step through the system is considered an element. Each element is given by a sequence of items separated by spaces and terminated by a semicolon. These items are a type code

number, a vary field, the physical parameter and optional labels. The type code number identifies the element (i.e., magnet, drift space, pole face rotation). A vary field allows the user to adjust the physical parameters of an element if the problem involves fitting. Physical parameters are quantities which describe the physical element. Optional labels assist in identifying beam elements and parameters in the output. A summary of TRANSPORT type codes is shown on page 77. [Ref. 13]

The initial objective in writing the input program will be to specify the beam line, establishing the central trajectory. The system to model by TRANSPORT is shown in Figure B-1. This system consists of two bending magnets and five drift lengths where

L_0 = initial drift length ,

L = effective pathlength through bending magnet ,

L_1 = drift length 1 ,

L_2 = drift length 2 ,

α = bending angle .

2. SAMPLE PROGRAM DEVELOPMENT [Ref. 13]

Figure B-2 is a sample input program that establishes the beam line of Figure B-1, assuming the initial drift space, L_0 equals zero. Refer to Figure B-2 for the remainder of this section.

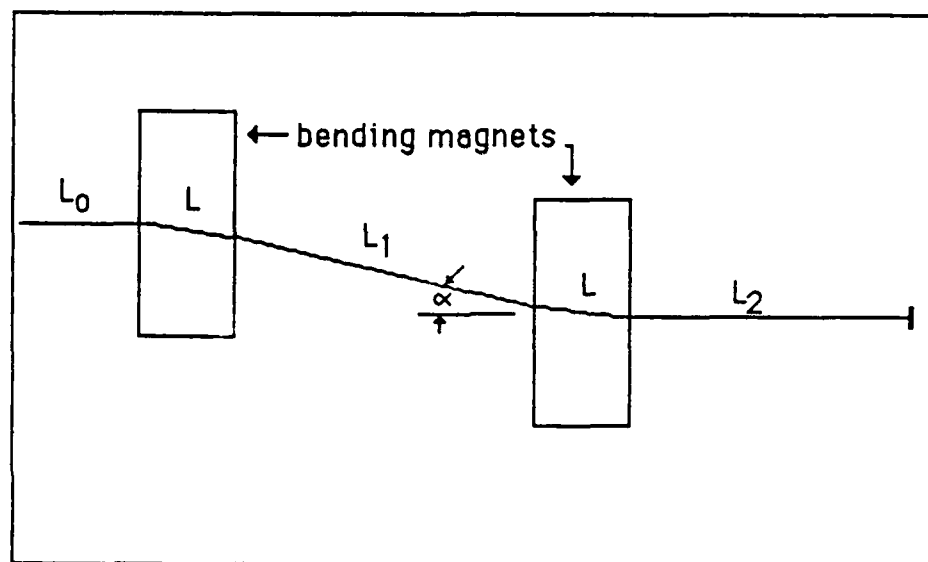


Figure B-1 System Configuration

```

(1)  'STANFORD MKIII IRFEL: REVISED 10/16/87'
0

(2)  (CARTESIAN COORDINATE SYSTEM: x,y,z)
13.  'COOR'      12.  ;

(3)  (SET UNITS/scaled units)
15.  'xymm'      1.   ' mm'      0.1  ;
15.  'EMeV'     11.   ' MeV'     0.001 ;
15.  'long'      8.   ' mm'     0.001 ;
15.  'leng'      5.   ' mm'     0.1  ;

(4)  (BEAM PARAMETERS at FIRST BENDING MAGNET POLE-FACE)
(NORMALIZED BEAM EMITTANCE: Enh=8mm-mrad, Env=4mm-mrad)
1.0  'BEAM'  1.0  0.1  1.0  0.05  .0005  0.0  40.0 ;
(monoenergetic beam)

(5)  16.      5.   5.0  ; (half-gap).
      (default value of K1=.5)

(6)  (FIRST BENDING MAGNET)
2.   0.   ;
4.   'BND1'  38.347  6.83175  0.  ;
2.   11.25  ;
13.  1.   ; (PRINT BEAM MATRIX)
13.  4.   ; (PRINT XFORM MATRIX)

(7)  (DRIFT SPACE #1)
3.   'DFT1'  327.03  ;
13.  1.   ;
13.  4.   ;

(8)  (SECOND BENDING MAGNET)
20.  180.  'LEFT' ; (std coord rot w/11.25 bend)
2.   11.25  ;
4.   'END2'  38.347  6.83175  0.  ;
2.   0.   ;
20.  -180.  ;
13.  1.   ;
13.  4.   ;

(9)  (DRIFT SPACE #2)
3.   'DFT2'  95.30  ;
13.  1.   ;
13.  4.   ;

(10) SENTINEL  ;

```

Figure B-2 Sample Input Program

The individual elements and there associated type codes will be explained in the succeeding paragraphs.

(1) 'STANFORD MKIII FEL: revised 10/16/87' is the arbitrary title of the sample input program. The zero immediately below the title indicates the start of a new problem.

(2) A cartesian coordinate system was chosen for the proposed experiment design problem. The coordinate system is established using the type code 13. The statement [13. 12. ;] will yield a beam line reference trajectory that will start at the origin and proceed along the positive z-axis. The y-axis will point up and the x-axis will point to the left. Statements enclosed by () are comment statements to assist in following the code.

(3) The scaling of units is accomplished via type code 15. All lengths in Figure B-1 are to be specified in millimeters and energy is to be specified in MeV. TRANSPORT has the standard set of units as shown on page 78. Conversion factors are applied to code digits 1, 11, 8, and 5 to establish an appropriate unit system. A summary of TRANSPORT type codes is found on page 77.

(4) The input beam, denoted by the type code 1, is specified in terms of its phase space and average momentum parameters. The phase space input is given in terms of the semi-axis of a six-dimensional beam ellipsoid representing the phase space variables x , θ , y , ϕ , l , and δ where

x = one-half the horizontal beam extent (1.0mm) ,
 θ = one-half the horizontal beam divergence (0.1mrad) ,
 y = one-half the vertical beam extent (1.0mm) ,
 ϕ = one-half the vertical beam divergence (.05mrad) ,
 l = one half the longitudinal beam extent (.0005mm) ,
 δ = one-half the momentum spread (0.0%) ,
 P = average momentum of the beam (40MeV/c) .

NOTE: The above units were scaled using type code 15.

(5) and (6) Bending magnet parameters are specified in terms of the wedge magnet, type code 4; pole-face rotation, type code 2; and a gap setting, type code 16. A wedge bending magnet implies that the central trajectory of the beam enters and exits perpendicularly to the pole face boundaries. A wedge magnet can be modified into a square edge magnet using the pole face rotation element on either the entrance or exit face of the magnet. The field boundaries for bending magnets are shown on page 73. To modify a wedge bending magnet into a square for a bend to the right, β_1 is set to zero and β_2 is set to 11.25 degrees. The pole face rotation type code 2. must immediately precede or immediately follow the bending magnet (type code 4.0). There are four first order parameters to be specified for the wedge magnet; the type code, the effective length of the central trajectory, the central field strength and the field gradient. The bending magnet equations and parameters for the system are listed below:

$L = \rho_0 \alpha$ where

L = effective pathlength through magnet ,

ρ_0 = bending radius; (195.30 mm) ,

α = bend angle; (11.25 degrees) ,

$L = (195.30\text{mm})(11.25\text{deg})(\text{rad}/180\text{deg}) = 38.347 \text{ mm} .$

(NOTE: To simulate a gradual variation of the fields at the ends of the bending magnets a fringing field element is provided.)

$B(0) = 33.356(P/\rho_0)$ where

$B(0)$ = central field strength ,

P = central momentum; (40 MeV/c) ,

$B(0) = 33.356(40\text{MeV/c})/195.30\text{mm} = 6.83175 \text{ kG} ,$

n = magnetic field gradient ($n = 0$ assumed).

Code [13. 1. ;] yields the printing of the current beam (o) matrix. Code [13. 4. ;] yields the printing of the current transformation matrix, R1. These codes will be addressed in the matrix formulation of TRANSPORT.

(7) and (9) A drift length (type code 3.0) is a field free region through which the beam passes. It is denoted by the type code and the effective drift length:

L_1 = drift length 1 (327.03 mm) ,

L_2 = drift length 2 (95.30 mm) .

(8) The second bending magnet differs from the first in that β_1 is set to 11.25 degrees and β_2 is set to zero degrees. In addition, a coordinate rotation element (type code 20.) is required to rotate the transverse coordinates x and y through an angle about the z -axis. A bend to the left

(looking in the direction of beam travel) is accomplished by rotating the x,y coordinates by 180 degrees.

(10) The word "sentinel" denotes the end of the input program.

3. MATRIX FORMULATION OF TRANSPORT [Ref. 13]

A. Phase Space Vector

At any specified position in the system an arbitrary charged particle is represented by a vector X , whose components are the positions, angles, and momentum of the particle with respect to the central trajectory. The X vector is represented:

$$X = \begin{bmatrix} x \\ \theta \\ y \\ \phi \\ l \\ \delta \end{bmatrix}$$

where

x = the horizontal displacement of the arbitrary ray with respect to the assumed central trajectory ,

θ = the angle this ray makes in the horizontal plane with respect to the assumed central trajectory ,

y = the vertical displacement of the ray with respect to the assumed central trajectory ,

ϕ = the vertical angle of the ray with respect to the central trajectory ,

l = the path length difference between the arbitrary ray and the central trajectory ,

δ = $\Delta P/P$; the fractional momentum deviation of the ray from the assumed central trajectory.

B. The Transfer Matrix R

The passage of a charged particle through an element (magnet, drift space, rotation, etc.) may be represented by Equation B-1:

$$X(1) = RX(0) , \quad (B-1)$$

where

$X(0)$ is the initial coordinate vector,

$X(1)$ is the final coordinate vector,

R is the transformation matrix of the element.

In a system of several magnets, pole face rotations, and drift spaces, R is replaced by the product matrix $R(t)$:

$$R(t) = R(n) \dots R(3)R(2)R(1) . \quad (B-2)$$

$R(t)$ is the product of the individual element matrices of the system. Equation B-3 represents the matrix equation for a system:

$$X_i(t) = \sum_{j=1}^6 R_{ij} X_j(0) , \quad (B-3)$$

where

$$X_1 = x ,$$

$$X_2 = \theta ,$$

$$\begin{aligned}
X_3 &= y, \\
X_4 &= \phi, \\
X_5 &= 1, \text{ and} \\
X_6 &= \delta.
\end{aligned}$$

This product matrix is automatically calculated by the program and is called TRANSFORM1. TRANSFORM1 can be printed when desired using the statement [13. 4. ;] (e.g., paragraph (6)). For static magnetic systems possessing midplane symmetry, the six simultaneous linear equations represented by Equation B-3 may be expanded in matrix form as [Ref. 14]:

$$\begin{bmatrix} x(t) \\ \theta(t) \\ y(t) \\ \phi(t) \\ 1(t) \\ \delta(t) \end{bmatrix} = \begin{bmatrix} R_{11} & R_{12} & 0 & 0 & 0 & R_{16} \\ R_{21} & R_{22} & 0 & 0 & 0 & R_{26} \\ 0 & 0 & R_{33} & R_{34} & 0 & 0 \\ 0 & 0 & R_{43} & R_{44} & 0 & 0 \\ R_{51} & R_{52} & 0 & 0 & 1 & R_{56} \\ 0 & 0 & 0 & 0 & 0 & 1 \end{bmatrix} \begin{bmatrix} x_0 \\ \theta_0 \\ y_0 \\ \phi_0 \\ 1_0 \\ \delta_0 \end{bmatrix}$$

The transformation is from an initial position $\tau = 0$ to a final position $\tau = t$ measured along the assumed central trajectory. The final coordinate vector $X(t)$ is the matrix product of the individual coordinate vector and the overall system transformation matrix. The individual R_{ij} elements of the matrix are dimensionally consistent with the input units specified in the transport code. The individual transformation matrices needed to represent the system of

Figure B-1 are shown on pages 74-76. It is desired to determine and plot $x(t)$ vs $l(t)$ for the overall system. Since the system is symmetric, $x(t)$ and $l(t)$ have no dependence upon y_0 or ϕ_0 , thus the general form of the transformation matrix is reduced to:

$$\begin{bmatrix} x(t) \\ \theta(t) \\ l(t) \\ \delta(t) \end{bmatrix} = \begin{bmatrix} R_{11} & R_{12} & 0 & R_{16} \\ R_{21} & R_{22} & 0 & R_{26} \\ R_{51} & R_{52} & 1 & R_{56} \\ 0 & 0 & 0 & 1 \end{bmatrix} \begin{bmatrix} x_0 \\ \theta_0 \\ l_0 \\ \delta_0 \end{bmatrix}.$$

The wedge bending magnet is reduced to:

$$\begin{bmatrix} \cos \alpha & \rho_0 \sin \alpha & 0 & \rho_0 (1 - \cos \alpha) \\ -h \sin \alpha & \cos \alpha & 0 & \sin \alpha \\ -\sin \alpha & -\rho_0 (1 - \cos \alpha) & 1 & -\rho_0 (\alpha - \sin \alpha) \\ 0 & 0 & 0 & 1 \end{bmatrix}$$

The pole face rotation matrix is reduced to:

$$\begin{bmatrix} 1 & 0 & 0 & 0 \\ (\tan \alpha) / \rho_0 & 1 & 0 & 0 \\ 0 & 0 & 1 & 0 \\ 0 & 0 & 0 & 1 \end{bmatrix}.$$

The drift space matrix is reduced to:

$$\begin{bmatrix} 1 & L & 0 & 0 \\ 0 & 1 & 0 & 0 \\ 0 & 0 & 1 & 0 \\ 0 & 0 & 0 & 1 \end{bmatrix}.$$

It is desired to determine the X matrix at various locations along the central trajectory. Figure B-3 denotes the system locations to be evaluated:

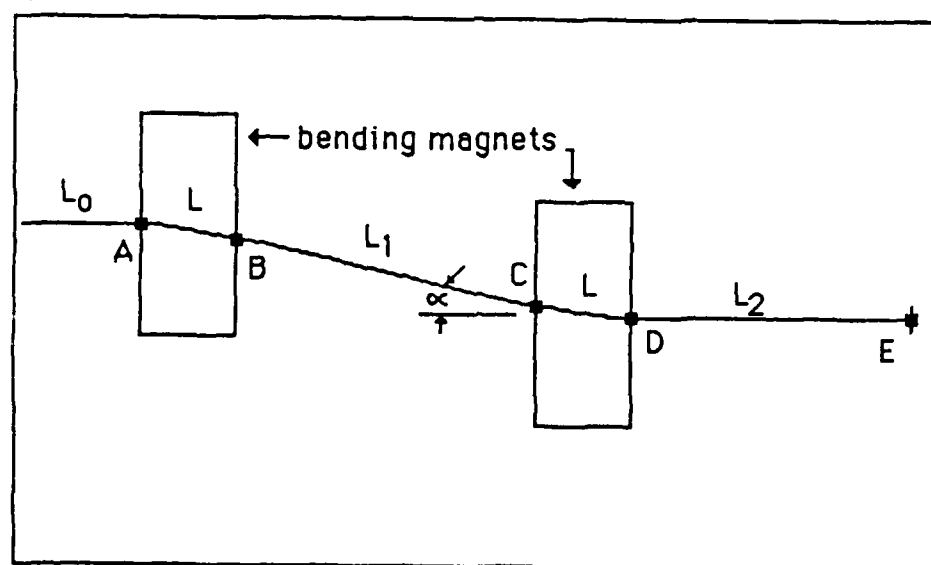


Figure B-3 System Configuration Evaluation Points

The matrix representation of $X_B(t)$ is the product of the pole face rotation matrix, wedge bending magnet matrix, and the initial coordinate vector:

$$\begin{bmatrix} x_B(t) \\ \theta_B(t) \\ l_B(t) \\ \delta_B(t) \end{bmatrix} = \begin{bmatrix} 1 & 0 & 0 & 0 \\ \tan \alpha / \rho_0 & 1 & 0 & 0 \\ 0 & 0 & 1 & 0 \\ 0 & 0 & 0 & 1 \end{bmatrix} \begin{bmatrix} \cos \alpha & \rho_0 \sin \alpha & 0 & \rho_0 (1 - \cos \alpha) \\ -\sin \alpha & \cos \alpha & 0 & \sin \alpha \\ -\sin \alpha & \rho_0 (1 - \cos \alpha) & 1 & -\rho_0 (\alpha - \sin \alpha) \\ 0 & 0 & 0 & 1 \end{bmatrix} \begin{bmatrix} x_0 \\ \theta_0 \\ l_0 \\ \delta_0 \end{bmatrix}$$

(pole face rotation) (wedge bending magnet)

The matrix product reduces to:

$$\begin{bmatrix} x_B(t) \\ \theta_B(t) \\ l_B(t) \\ \delta_B(t) \end{bmatrix} = \begin{bmatrix} \cos \alpha & \rho_0 \sin \alpha & 0 & \rho_0 (1 - \cos \alpha) \\ 0 & 1 / \cos \alpha & 0 & \tan \alpha \\ -\sin \alpha & -\rho_0 (1 - \cos \alpha) & 1 & -\rho_0 (\alpha - \sin \alpha) \\ 0 & 0 & 0 & 1 \end{bmatrix} \begin{bmatrix} x_0 \\ \theta_0 \\ l_0 \\ \delta_0 \end{bmatrix}$$

The matrix representation of $X_C(t)$ is $X_B(t)$ multiplied by the first drift space matrix:

$$\begin{bmatrix} x_C(t) \\ \theta_C(t) \\ l_C(t) \\ \delta_C(t) \end{bmatrix} = \begin{bmatrix} 1 & L_1 & 0 & 0 \\ 0 & 1 & 0 & 0 \\ 0 & 0 & 1 & 0 \\ 0 & 0 & 0 & 1 \end{bmatrix} \begin{bmatrix} \cos \alpha & \rho_0 \sin \alpha & 0 & \rho_0 (1 - \cos \alpha) \\ 0 & 1 / \cos \alpha & 0 & \tan \alpha \\ -\sin \alpha & -\rho_0 (1 - \cos \alpha) & 1 & -\rho_0 (\alpha - \sin \alpha) \\ 0 & 0 & 0 & 1 \end{bmatrix} \begin{bmatrix} x_0 \\ \theta_0 \\ l_0 \\ \delta_0 \end{bmatrix}$$

(first drift) $X_B(t)$

The matrix product reduces to:

$$\begin{bmatrix} x_C(t) \\ \theta_C(t) \\ l_C(t) \\ s_C(t) \end{bmatrix} = \begin{bmatrix} \cos \alpha & \rho_0 \sin \alpha + L_1 / \cos \alpha & 0 & \rho_0 (1 - \cos \alpha) + L_1 \tan \alpha \\ 0 & 1 / \cos \alpha & 0 & \tan \alpha \\ -\sin \alpha & -\rho_0 (1 - \cos \alpha) & 1 & -\rho_0 (\alpha - \sin \alpha) \\ 0 & 0 & 0 & 1 \end{bmatrix} \begin{bmatrix} x_0 \\ \theta_0 \\ l_0 \\ s_0 \end{bmatrix}$$

The matrix representation of $X_D(t)$ includes a coordinate rotation which will in effect bend the beam to the left. In matrix form this is represented by changing the bending radius and bending angle to its negative value (i.e., $\rho_0 \rightarrow -\rho_0$, $\alpha \rightarrow -\alpha$). The wedge bending matrix for a bend to the left is modified as shown :

$$\begin{bmatrix} \cos \alpha & \rho_0 \sin \alpha & 0 & \rho_0 (1 - \cos \alpha) \\ -\sin \alpha & 1 / \cos \alpha & 0 & \tan \alpha \\ \sin \alpha & -\rho_0 (1 - \cos \alpha) & 1 & -\rho_0 (\alpha - \sin \alpha) \\ 0 & 0 & 0 & 1 \end{bmatrix}$$

The pole face rotation matrix retains its identical form because $\tan(-\alpha) = -\tan(\alpha)$. Multiplying $X_C(t)$ by the pole face rotation matrix and the wedge bending magnet matrix yields:

$$\begin{bmatrix} x_D(t) \\ \theta_D(t) \\ l_D(t) \\ \delta_D(t) \end{bmatrix} = \begin{bmatrix} 1 & 2\rho_0 \tan \alpha + L_1 / \cos^2 \alpha & 0 & Z1 \\ 0 & 1 & 0 & 0 \\ 0 & Z2 & 1 & Z3 \\ 0 & 0 & 0 & 1 \end{bmatrix} \begin{bmatrix} x_0 \\ \theta_0 \\ l_0 \\ \delta_0 \end{bmatrix}$$

where:

$$Z1 = -2\rho_0 + 2\rho_0 / \cos \alpha + L_1 \sin \alpha / \cos^2 \alpha ,$$

$$Z2 = Z1 ,$$

$$Z3 = -2\rho_0 \alpha + 2\rho_0 \tan \alpha + L_1 \tan^2 \alpha .$$

The matrix representation of $X_E(t)$ is $X_D(t)$ multiplied by the second drift space matrix:

$$\begin{bmatrix} x_E(t) \\ \theta_E(t) \\ l_E(t) \\ \delta_E(t) \end{bmatrix} = \begin{bmatrix} 1 & Z4 & 0 & Z5 \\ 0 & 1 & 0 & 0 \\ 0 & Z6 & 1 & Z7 \\ 0 & 0 & 0 & 1 \end{bmatrix} \begin{bmatrix} x_0 \\ \theta_0 \\ l_0 \\ \delta_0 \end{bmatrix}$$

where:

$$Z4 = 2\rho_0 \tan \alpha + L_1 / \cos^2 \alpha + L_2 ,$$

$$Z5 = -2\rho_0 + 2\rho_0 / \cos \alpha + L_1 \sin \alpha / \cos^2 \alpha ,$$

$$Z6 = Z5 ,$$

$$Z7 = -2\rho_0 \alpha + 2\rho_0 \tan \alpha + L_1 \tan^2 \alpha .$$

In equation form, the matrix products are represented as:

$$x_B(t) = (\cos \alpha) x_O + (\rho_O \sin \alpha) \theta_O + \rho_O (1 - \cos \alpha) \delta_O \quad (M-1)$$

$$\theta_B(t) = (1/\cos \alpha) \theta_O + (\tan \alpha) \delta_O \quad (M-2)$$

$$l_B(t) = (-\sin \alpha) x_O - \rho_O (1 - \cos \alpha) \theta_O + l_O - \rho_O (\alpha - \sin \alpha) \delta_O \quad (M-3)$$

$$\delta_B(t) = \delta_O \quad (M-4)$$

$$x_C(t) = (\cos \alpha) x_O + (\rho_O \sin \alpha + L_1/\cos \alpha) \theta_O + [\rho_O (1 - \cos \alpha) + L_1 \tan \alpha] \delta_O \quad (M-5)$$

$$\theta_C(t) = (1/\cos \alpha) \theta_O + (\tan \alpha) \delta_O \quad (M-6)$$

$$l_C(t) = (-\sin \alpha) x_O - \rho_O (1 - \cos \alpha) \theta_O + l_O - \rho_O (\alpha - \sin \alpha) \delta_O \quad (M-7)$$

$$\delta_C(t) = \delta_O \quad (M-8)$$

$$x_C(t) = x_B(t) + L_1 \theta_B(t) \quad (M-5A)$$

$$\theta_C(t) = \theta_B(t) \quad (M-6A)$$

$$l_C(t) = l_B(t) \quad (M-7A)$$

$$\delta_C(t) = \delta_B(t) \quad (M-8A)$$

$$x_D(t) = x_O + (2 \rho_O \tan \alpha + L_1/\cos^2 \alpha) \theta_O + (-2 \rho_O + 2 \rho_O/\cos \alpha + L_1 \sin \alpha/\cos^2 \alpha) \delta_O \quad (M-9)$$

$$\theta_D(t) = \theta_O \quad (M-10)$$

$$l_D(t) = (-2 \rho_O + 2 \rho_O/\cos \alpha + L_1 \sin \alpha/\cos^2 \alpha) \theta_O + l_O + (-2 \rho_O \alpha + 2 \rho_O \tan \alpha + L_1 \tan^2 \alpha) \delta_O \quad (M-11)$$

$$\delta_D(t) = \delta_O \quad (M-12)$$

$$x_D(t) = (1/\cos \alpha) x_C(t) + (\rho_0 \sin \alpha) \theta_C(t) - \rho_0 (1 - \cos \alpha) \delta_C(t) \quad (M-9A)$$

$$\theta_D(t) = (\cos \alpha) \theta_C(t) - (\sin \alpha) \delta_C(t) \quad (M-10A)$$

$$l_D(t) = (\tan \alpha) x_C(t) + \rho_0 (1 - \cos \alpha) \theta_C(t) + l_C - \rho_0 (\alpha - \sin \alpha) \delta_C(t) \quad (M-11A)$$

$$\delta_D(t) = \delta_C(t) \quad (M-12A)$$

$$x_E(t) = x_0 + (2\rho_0 \tan \alpha + L_1/\cos^2 \alpha + L_2) \theta_0 + (-2\rho_0 + 2\rho_0/\cos \alpha + L_1 \sin \alpha/\cos^2 \alpha) \delta_0 \quad (M-13)$$

$$\theta_E(t) = \theta_0 \quad (M-14)$$

$$l_E(t) = (-2\rho_0 + 2\rho_0/\cos \alpha + L_1 \sin \alpha/\cos^2 \alpha) \theta_0 + l_0 + (-2\rho_0 \alpha + 2\rho_0 \tan \alpha + L_1 \tan^2 \alpha) \delta_0 \quad (M-15)$$

$$\delta_E(t) = \delta_0 \quad (M-16)$$

$$x_E(t) = x_D(t) + L_2 \theta_D(t) \quad (M-13A)$$

$$\theta_E(t) = \theta_D(t) \quad (M-14A)$$

$$l_E(t) = l_D(t) \quad (M-15A)$$

$$\delta_E(t) = \delta_D(t) \quad (M-16A)$$

C. Beam Matrix

The phase ellipse beam (sigma) matrix is used to inform the user of the beam parameters at any location in the system. The beam matrix will represent the bundle of particles or rays constituting the phase space of the input beam at desired locations in the system. Particles of the beam are assumed to lie within the boundaries of the ellipsoid with each point within the ellipsoid representing a possible ray. The equation of an n-dimensional ellipsoid may be written in matrix form as:

$$X(0)^T \sigma(0)^{-1} X(0) = 1 , \quad (B-4)$$

where:

$X(0)^T$ = transpose of coordinate vector $X(0)$,

$\sigma(0)$ = a real positive definite, symmetric matrix.

As a particle passes through the system, it undergoes the matrix transformation of Equation B-1. Combining this transformation with the equation of the initial ellipsoid and using $RR^{-1} = I$:

$$X(0)^T (R^T R^{-1}) \sigma(0)^{-1} (R^{-1} R) X(0) = 1 . \quad (B-5)$$

Equation B-5 can be rewritten as:

$$[RX(0)]^T [R\sigma(0)R^T]^{-1} [RX(0)] = 1 . \quad (B-6)$$

The equation of the new ellipsoid after the transformation becomes:

$$X(1)^T \sigma(1)^{-1} X(1) = 1 , \quad (B-7)$$

where:

$$\sigma(1) = R\sigma(0)R^T . \quad (B-8)$$

Thus the beam may be represented at any point in the system by Equation B-8. Note: $\sigma(0)$ is the input beam phase space specified by the user. The beam matrix is printed using the statement [13. 1. ;]. The projection of the semi-axis of the ellipsoid upon each of its six coordinate axes is printed in a vertical array, and the correlations among these components are printed in a triangular array. The phase ellipse beam matrix in the printed output form is shown in Figure B-4.

			x	θ	y	ϕ	z
x	$\sqrt{\sigma(11)}$	CM					
θ	$\sqrt{\sigma(22)}$	MR	r(21)				
y	$\sqrt{\sigma(33)}$	CM	r(31)	r(32)			
ϕ	$\sqrt{\sigma(44)}$	MR	r(41)	r(42)	r(43)		
z	$\sqrt{\sigma(55)}$	CM	r(51)	r(52)	r(53)	r(54)	
δ	$\sqrt{\sigma(66)}$	PC	r(61)	r(62)	r(63)	r(64)	r(65)

where:
$$r(ij) = \frac{\sigma(ij)}{[\sigma(ii)\sigma(jj)]^{\frac{1}{2}}}$$

As a result of the fact that the σ matrix is positive definite, the $r(ij)$ satisfy the relation

$$|r(ij)| \leq 1.$$

Figure B-4 Beam matrix

(Note: units will be labeled as specified by type code 15.)

The individual sigma elements are defined:

$\sqrt{\sigma}$ (11) = x_{\max} = the maximum half-width of the beam envelope in the x(bend)-plane at the point of the printout,

$\sqrt{\sigma}$ (22) = θ_{\max} = the maximum half-angular divergence of the beam envelope in the x(bend) plane,

$\sqrt{\sigma}$ (33) = y_{\max} = the maximum half-height of the beam envelope,

$\sqrt{\sigma}$ (44) = ϕ_{\max} = the maximum half-angular divergence of the beam envelope in the y(non-bend) plane,

$\sqrt{\sigma}$ (55) = l_{\max} = one-half the longitudinal extent of the bunch of particles,

$\sqrt{\sigma}$ (66) = δ = the half-width $1/2(\Delta P/P)$ of the momentum interval being transmitted by the system.

Note: the units appearing next to the $\sqrt{\sigma}$ (ii) in the TRANSPORT printout are the units chosen for coordinates x, θ y, ϕ , l, and δ respectively.

An example of the (x, θ) plane ellipse is illustrated in Figure B-5.

Consider a two dimensional (x, θ) plane projection of the general 6-dimensional ellipsoid. Let:

$$\sigma = \begin{bmatrix} \sigma_{11} & \sigma_{21} \\ \sigma_{21} & \sigma_{22} \end{bmatrix}$$

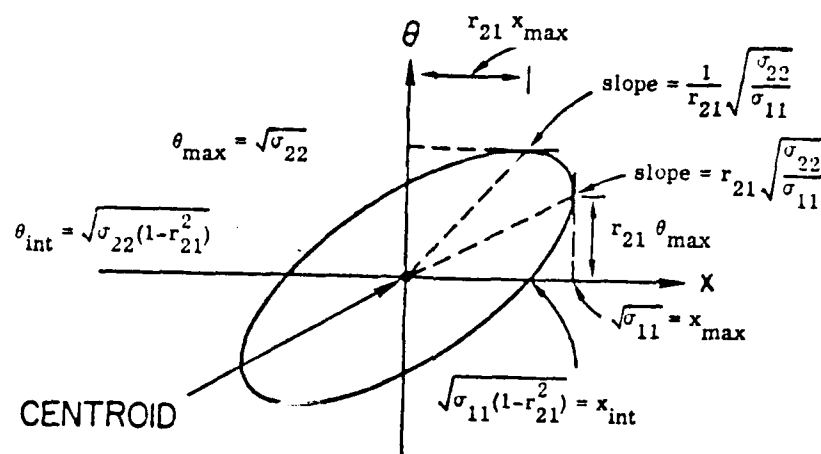


Figure B-5 A Two Dimensional Beam Phase Ellipse

be a real, positive definite, symmetric matrix. The inverse of the σ -matrix exists and is defined by:

$$\sigma^{-1} = 1/\epsilon^2 \begin{bmatrix} \sigma_{22} & -\sigma_{21} \\ -\sigma_{21} & \sigma_{11} \end{bmatrix}$$

where ϵ^2 is the determinant of .

The two-dimensional coordinate vector and its transpose are represented by:

$$X = \begin{bmatrix} x \\ \theta \end{bmatrix} ; \quad X^T = (x, \theta) .$$

The expansion of the matrix equation

$$X^T \sigma^{-1} X = 1$$

is the equation of an ellipse, therefore

$$\sigma_{22}x^2 - 2\sigma_{21}x\theta + \sigma_{11}\theta^2 = \epsilon^2 = \det \sigma.$$

The area of the ellipse is given by:

$$A = \pi (\det \sigma)^{1/2} = \pi x_{\max} \theta_{\min} = \pi x_{\min} \theta_{\max} = \pi \epsilon.$$

The correlation between x and θ (the orientation of the ellipse) depends on the off diagonal term σ_{21} . This correlation is defined as:

$$r_{21} = r_{12} = \frac{\sigma_{21}}{\sqrt{\sigma_{11}\sigma_{22}}}$$

The correlation, r , measures the tilt of the ellipse and the intersection of the ellipse with the coordinate axis. The beam ellipse in the (x, θ) plane will be valuable in the analysis of the beam divergence at various points in the system and also in the fact that it reveals the change in the longitudinal extent of the beam via element $\sqrt{\sigma}$ (55).

4. INSTALLATION OF TRANSPORT ON THE IBM PC [Ref. 15]

The following requirements and procedures are necessary for the loading and running of TRANSPORT:

Requirements:

- config.sys file must have files >= 15; buffers >= 15.
- disk set A containing .EXE and .BAT files in DOS/BACKUP
- 640K memory
- hard disk; 10M-byte or larger

Procedures:

- move to the C directory: C:[ENTER]
- create a TEMPO subdirectory: MD\TEMPO[ENTER]
- move to the TEMPO subdirectory: CD\TEMPO[ENTER]
- RESTORE .EXE and .BAT files: RESTORE A: C:[ENTER]
(insert disk #1 and #2 as directed)
- move to the C directory: CD\C:[ENTER]
- create a TRANS subdirectory: MD\TRANS[ENTER]
- move to the TEMPO subdirectory: CD\TEMPO[ENTER]
- copy files from TEMPO to TRANS: copy *.* \TRANS[ENTER]
- delete files from TEMPO subdirectory: del *.*[ENTER]
- move to the C directory: CD\C:[ENTER]
- remove TEMPO subdirectory: RD\TEMPO[ENTER]

Limitations:

- the PC version of TRANSPORT will allow for 1000 elements and 4500 data values
- accuracy is four significant figures

To run TRANSPORT:

- TRANSGO.BAT is the command file to run TRANS.EXE
- type the following:

TRANSGO FILE1 FILE2 FILE3

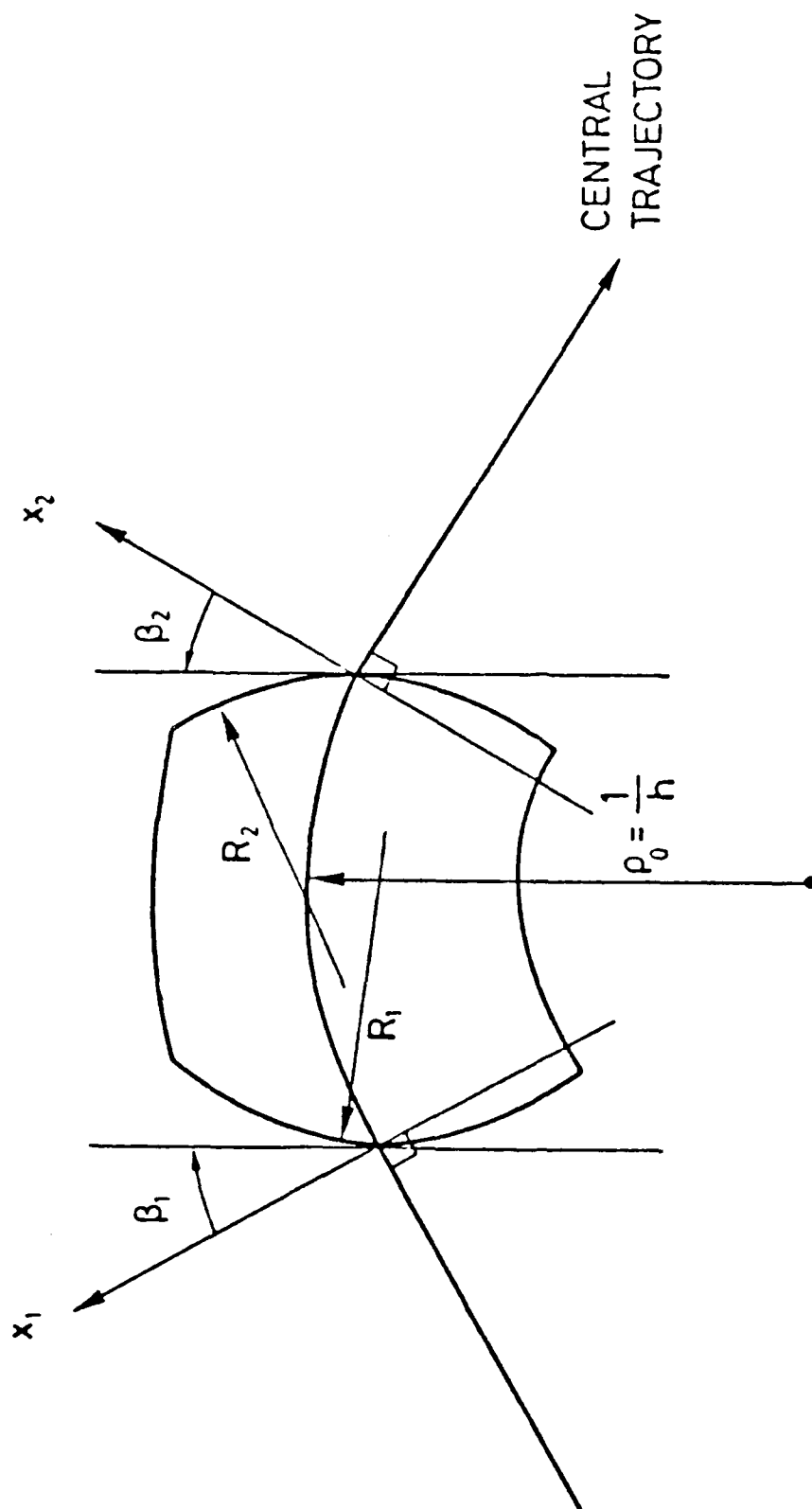
FILE1: input data file name (users file name)

FILE2: output print file name (users file name)

FILE3: output summary file name (users file name)

- example: TRANSGO MK3FELA MK3FELA.OUT MK3FELA.JNK[ENTER]

- * Note: TRANSPORT is currently loaded in the IBM PCs in the Physics Library and Physics Department Office under the subdirectory C:\TRANS. X. Maruyama currently holds the TRANSPORT software on 5-1/4 disks.



FIELD BOUNDARIES FOR BENDING MAGNETS

The TRANSPORT sign conventions for x , β , R and h are all positive as shown in the figure. The positive y direction is out of the paper. Positive β 's imply transverse focusing. Positive R 's (convex curvatures) represent negative sextupole components of strength $S = (-h/2R) \sec^3 \beta$. (See SLAC-75, page 71.)

First-order wedge bending magnet matrix

$\cos k_x L$	$\frac{1}{k_x} \sin k_x L$	0	0	0	$\frac{h}{k_x^2} (1 - \cos k_x L)$
$-k_x \sin k_x L$	$\cos k_x L$	0	0	0	$\frac{h}{k_x} \sin k_x L$
0	0	$\cos k_y L$	$\frac{i}{k_y} \sin k_y L$	0	0
0	0	$-k_y \sin k_y L$	$\cos k_y L$	0	0
$-\frac{h}{k_x} \sin k_x L$	$-\frac{h}{k_x^2} (1 - \cos k_x L)$	0	0	1	$-\frac{h^2}{k_x^3} (k_x L - \sin k_x L)$
0	0	0	0	0	1

Definitions: $h = 1/\rho_0$, $k_x^2 = (1-n)h^2$, $k_y^2 = nh^2$

$\alpha = hL$ = the angle of bend

L = path length of the central trajectory.

Pole-face rotation matrix

The first-order R matrix for a pole-face rotation used in a TRANSPORT calculation is as follows:

$$R = \begin{bmatrix} 1 & 0 & 0 & 0 & 0 & 0 \\ \frac{\tan \beta}{\rho_0} & 1 & 0 & 0 & 0 & 0 \\ 0 & 0 & 1 & 0 & 0 & 0 \\ 0 & 0 & -\frac{\tan(\beta-\psi)}{\rho_0} & 1 & 0 & 0 \\ 0 & 0 & 0 & 0 & 1 & 0 \\ 0 & 0 & 0 & 0 & 0 & 1 \end{bmatrix}$$

R =

Definitions: β = angle of rotation of pole face (see figure on following page for sign convention of β)

ρ_0 = bending radius of central trajectory

g = total gap of magnet

ψ = correction term resulting from spatial extent of fringing fields^{**}).

where

$$\psi = K_1 \left(\frac{g}{\rho_0} \right) \left(\frac{1 + \sin^2 \beta}{\cos \beta} \right) \left[1 - K_1 K_2 \left(\frac{g}{\rho_0} \right) \tan \beta \right]^*$$

Drift space matrix

The first-order R matrix for a drift space is as follows:

$$\begin{pmatrix}
 1 & L & 0 & 0 & 0 & 0 \\
 0 & 1 & 0 & 0 & 0 & 0 \\
 0 & 0 & 1 & L & 0 & 0 \\
 0 & 0 & 0 & 0 & 1 & 0 \\
 0 & 0 & 0 & 0 & 0 & 1 \\
 0 & 0 & 0 & 0 & 0 & 1
 \end{pmatrix}$$

where

L = the length of the drift space.

The dimensions of L are those chosen for longitudinal length via

15. 8. ' , ; type code entry (if used) preceding the BEAM (type code 1.0)
 card. If no 15. 8. entry is made, the units of L will automatically be
 in metres (standard TRANSPORT units).

Table 1: Summary of TRANSPORT type codes

PHYSICAL ELEMENT	TYPE CODE	2nd ENTRY	3rd ENTRY	4th ENTRY	5th ENTRY	6th ENTRY	7th ENTRY	8th ENTRY	9th ENTRY
BEAM r.m.s. ADDITION TO BEAM ENVELOPE	1.vvvvvv0 1.vvvvvv00	x(cm) Δx(cm)	0(mr) Δθ(mr)	y(cm) Δy(cm)	0(mr) Δθ(mr)	z(cm) Δz(cm)	Δ(1-100%) Δδ(percent)	Δp Δp (GeV/c)	0
INLET FACE ROTATION	2.v	ANGLE OF ROTATION (degrees)							
DRIFT	3.v	LENGTH (metres)							
BENDING MAGNET	4.vvv	LENGTH (metres)	FIELD (kG)	FIELD GRADIENT (n-value)					
QUADRUPOLE	5.vv0	LENGTH (metres)	FIELD (kG)	HALF-APERTURE (cm)					
TRANSFORM 1 UPDATE	6.0	0.0	1.0						
TRANSFORM 2 UPDATE	6.0	0.0	2.0						
BEAM CENTERED SHIFT	7.vvvvvvv	SHIFT (x)(cm)	SHIFT (θ) (mr)	SHIFT (y)(cm)	SHIFT (θ)(mr)	SHIFT (z)(cm)	SHIFT (δ)(percent)		
ALIGNMENT TOLERANCE	8.vvvvvv0	DISPLACEMENT (x)(cm)	ROTATION (θ)(mr)	DISPLACEMENT (y)(cm)	ROTATION (θ)(mr)	DISPLACEMENT (z)(cm)	ROTATION (α)(mr)	Q-TIME NUMBER	
REPEAT CONTROL	9.0	NUMBER OF REPEATS							
FITTING CONSTRAINTS	10.0	+1	J	DESIRED VALUE OF (I,J) MATRIX ELEMENTS	ACCURACY OF FIT				

Note: +1 is used for fitting a beam (σ) matrix element. -1 is used for fitting an R1 matrix element.
- (1 + 20) is used for fitting an R2 matrix element.

ACCELERATOR	11.0	LENGTH (metres)	E (energy gain) (GeV)	θ (phase lag) (degrees)	WAVELENGTH (cm)				
BEAM (Rotated Ellipse)	12.0	THE FIFTEEN CORRELATIONS AMONG THE SIX ELEMENTS (this entry must be preceded by a type code 1.0 entry.)							
INPUT/OUTPUT OPTIONS	13.0	CONTROL CODE NUMBER							
ARBITRARY R MATRIX	14.vvvvvv0	R(J,1)	R(J,2)	R(J,3)	R(J,4)	R(J,5)	R(J,6)	J	
UNITS CONTROL (Transport Dimensions)	15.0	CODE	UNIT SYMBOL	SCALE FACTOR (if required)					
QUADRATIC TERM OF BENDING FIELD	16.0v	1.0	$c(1) = B(\frac{1}{\rho})^2$	a, in units of transverse length (cm)					
MASS OF PARTICLES IN BEAM	16.0	3.0	M/m (dimensionless)	m = mass of electron					
HALF-APERTURE OF BENDING MAGNET IN x-PLANE	16.0	4.0	w/2 (cm)						
HALF-APERTURE OF BENDING MAGNET IN y-PLANE (gap)	16.0	5.0	g/2 (cm)						
LENGTH OF SYSTEM	16.0	6.0	L (metres)						
FRINGE FIELD COR- RELATION COEFFICIENT	16.0	7.0	K ₁ (dimensionless)						
FRINGE FIELD COR- RELATION COEFFICIENT	16.0	8.0	K ₂ (dimensionless)						
CURVATURE OF ENTRANCE FACE OF BENDING MAGNET	16.0v	12.0	(1/R ₁) (1/metres)						
CURVATURE OF EXIT FACE OF BENDING MAGNET	16.0v	13.0	(1/R ₂) (1/metres)						
FOCAL PLANE ROTATION	16.0	15.0	Angle of focal plane rotation (degrees). See type code 16.0 for details.						
INITIAL BEAM LINE x-COORDINATE	16.0v	16.0	x ₀						
INITIAL BEAM LINE y-COORDINATE	16.0v	17.0	y ₀						
INITIAL BEAM LINE z-COORDINATE	16.0v	18.0	z ₀						
INITIAL BEAM LINE HORIZONTAL ANGLE	16.0v	19.0	θ ₀						
INITIAL BEAM LINE VERTICAL ANGLE	16.0v	20.0	φ ₀						
SIXTH-ORDER CALCULATIONS	17.0								
SEXTUPOLE	18.0v	LENGTH (metres)	FIELD (kG)	HALF-APERTURE (cm)					
SOLENOID	19.vv	LENGTH (metres)	FIELD (kG)						
BEAM ROTATION	20.v	ANGLE OF ROTATION (degrees)							
SPRAY FIELD	21.0	See later section of report.							

Note: The v's following the type codes indicate the parameters which may be varied. See section under type code 10.0 for a detailed explanation of Vary Codes. The units are standard TRANSPORT units (as shown) unless changed via type code 15.0 entries.

The various units that may be changed are:

Code Digit	Quantity	Standard TRANSPORT Unit	Symbols used in SLAC-75
1.0	horizontal and vertical trans- verse dimensions, magnet apertures, and misalignment displacements	cm	x,y
2.0	horizontal and vertical angles and misalignment rotation angles	mr	θ, ϕ
3.0	vertical beam extent (only) ^{*)} and bending magnet gap height	cm	y
4.0	vertical beam divergence ^{*)} (only)	mr	ϕ
5.0	pulsed beam length and wave length in accelerator	cm	l
6.0	momentum spread	percent (PC)	δ
7.0	bend, pole face rotation, and coordinate layout angles	degrees (DEG)	
8.0	length (longitudinal) of ele- ments, layout coordinates, and bending magnet pole face curvatures	metres (M)	t
9.0	magnetic fields	kG	B
10.0	mass	electron mass	m
11.0	momentum and energy gain in accelerator section	GeV/c GeV	p(0) ΔE

*) These codes should not be used if the coordinate rotation (20.0) type code is used anywhere in the system.

LIST OF REFERENCES

1. Buskirk, Fred R., Xavier K. Maruyama and John Neighbours, Naval Postgraduate School Technical Report NPS 61-86-013, Radiation Produced by the Modulated Beam of the Free Electron Laser, pps. 1-21, June 1986.
2. Rule, D.W., and R.B. Fiorito, Naval Surface Weapons Center Technical Report TR84-134, "The Use of Transition Radiation as a Diagnostic for Intense Beams", pps. 1-35, July 1984.
3. Sessler, Andrew M., and Douglas Vaughan, "Free Electron Lasers," American Scientist, v. 75, pp. 34-41, January-February 1987.
4. Colson, W.B., and A.M. Sessler, "Free Electron Lasers," Annual Review of Nuclear Particle Science, v. 35, pp. 25-54, 1985.
5. Brau, Charles A., "Free Electron Lasers," Los Alamos National Laboratory, Los Alamos, New Mexico, pp. 91-99, 1983 (PREPRINT).
6. Stolovy, G., W. Wadensweiler, J.M.J. Madey, S. Benson, "High Quality Hybrid Wiggler for the Infrared FEL and Coherent Harmonic Generation," High Energy Physics Laboratory, Stanford University, Stanford, California, 94305, unpublished.
7. Frank, I.M. et al., "Radiation of a Uniformly Moving Electron due to its Transition from a Medium into Another," Journal of Physics, v. 9, no. 5, 1945.
8. Smith, T.I., H.A. Schwettman, R. Rohatgi, Y. LaPierre, and J. Edighoffer, "Development of the SCA/FEL for Use in Biomedical and Material Science Experiments," Free Electron Lasers-Proceedings from the Eighth International Free Electron Laser Conference, Glasgow, United Kingdom, 1-5 Sept 1986, North-Holland Physics Publishing-Amsterdam.
9. Maruyama, Xavier K., Samuel Penner, Cha-Mei Tang and Phillip Sprangle, "Proposal for a FEL Driven by the NBS CW Microtron," Free Electron Lasers-Proceedings from the Eighth International Free Electron Laser Conference, Glasgow, United Kingdom, 1-5 Sept 1986, North-Holland Physics Publishing-Amsterdam.

10. Penner, Samuel and E. Lindstrom, National Bureau of Standards Design Note #4, "Electron Beam Transport Design," 7 July 1987.
11. Banford, A.P., The Transport of Charged Particle Beams. London, France: E&F.N. Spon Limited, 1966.
12. Benson, Steve, personal conversations, High Energy Physics Laboratory, Stanford University, Stanford, California, April-May 1987.
13. Carey, David, Stanford Linear Accelerator Center SLAC-91, Rev. 2, "TRANSPORT-A Computer Program for Designing Charged Particle Beam Systems," May 1977.
14. Brown, Karl L. and Sam K. Howry, Stanford Linear Accelerator Center SLAC-91, "TRANSPORT/360-A Computer Program for Designing Charged Particle Beam Transport Systems," July 1970.
15. Colman, Judith, "The Use of the IBM-PC Computer in Accelerator Design Calculations," Neutral Beam Division, Brookhaven National Laboratory, Upton, N.Y. 1973.

INITIAL DISTRIBUTION LIST

	No. Copies
1. Library, Code 0142 Naval Postgraduate School Monterey, CA 93943-5000	2
2. Physics Library, Code 61 Department of Physics Naval Postgraduate School Monterey, CA 93943-5000	2
3. Professor F. R. Buskirk, Code 61Bs Department of Physics Naval Postgraduate School Monterey, CA 93943-5000	5
4. Professor X. K. Maruyama, Code 61Mx Department of Physics Naval Postgraduate School Monterey, CA 93943-5000	5
5. Professor J. R. Neighbours, Code 61Nb Department of Physics Naval Postgraduate School Monterey, CA 93943-5000	5
6. Dr. Steven Benson High Energy Physics Laboratory Stanford University Stanford, CA 94305	2
7. Dr. Arthur Paul Lawrence Livermore National Laboratory Bldg. 5475, Mail L626 Livermore, CA 94550	1
8. Dr. Tom Knight Stanford Linear Accelerator Center Stanford, CA 94025	1
9. Dr. Richard Helm Stanford Linear Accelerator Center Stanford, CA 94025	1
10. LT Jack E. Joynson Department Head Class #102 SWOSCOLCOM NETC Newport, RI 02841-5000	5

- | | | |
|-----|---|---|
| 11. | LT Eric L. Sweigard
Department Head Class #102
SWOSCOLCOM
NETC Newport, RI 02841-5000 | 1 |
| 12. | Mr. Donald S. Snyder, Code 61
Department of Physics
Naval Postgraduate School
Monterey, CA 93943-5000 | 1 |
| 13. | Dr. Melvin A. Piestrup
Adelphi Technology
532 Emerson Street
Palo Alto, CA 94301 | 1 |
| 14. | Mr. Charles G. Karros
550 Harbor Road
Bricktown, NJ 08724 | |
| 15. | Defense Technical Information Center
Cameron Station
Alexandria, VA 22304-6145 | 2 |
| 16. | LT W. Fritchie
PMW 145
SPAWAR
Washington, DC 20363-5100 | 1 |
| 17. | Defense Advanced Research Project Agency
ATTN: MAJ George P. Lasche
1400 Wilson Blvd.
Arlington, VA 22209 | 1 |
| 18. | Dr. V. L. Granatstein
Electrical Engineering Dept.
University of Maryland
College Park, MD 20742 | 1 |
| 19. | Lawrence Livermore National Laboratory
University of California
ATTN: Dr. William M. Fawley
P. O. Box 808
Livermore, CA 94550 | 1 |
| 20. | Dr. Joseph Mack
M4, M.S. P-940
Los Alamos National Laboratory
Los Alamos, NM 87545 | 1 |

21. Naval Surface Weapons Center 3
White Oak Laboratory
ATTN: Dr. Han S. Uhm (R41)
Dr. Ralph Fiorito (R41)
Dr. Donald Rule (R41)
22. CAPT. Kurt Stevens 1
AFTAC/TX OP
Patrick AFB
Patrick, FL 32925
23. Dr. Kenneth Struve 1
Lawrence Livermore National Laboratory
P. O. Box 808
Livermore, CA 94550
24. MAJ Edward Pogue 1
SD10-DE
Pentagon, Room 1E-800
Washington, DC 20301-7100
25. LCDR E. Turner 1
PMW 145
SPAWAR
Washington, DC 20363-5100

END

DATE

FILMED

8-88

DTIC